8700–8718 *Nucleic Acids Research, 2022, Vol. 50, No. 15* *Published online 29 July 2022*
https://doi.org/10.1093/nar/gkac645

FACT subunit SUPT16H associates with BRD4 and contributes to silencing of interferon signaling

Dawei Zhou[1], Zhenyu Wu[1,2], Jun-Gyu Park[3], Guillaume N. Fiches[1], Tai-Wei Li[1], Qin Ma[2], Huachao Huang[4], Ayan Biswas[1,5], Luis Martinez-Sobrido[3], Netty G. Santoso[1,*] and Jian Zhu[1,*]

[1]Department of Pathology, The Ohio State University Wexner Medical Center, Columbus, OH 43210, USA, [2]Department of Biomedical Informatics, The Ohio State University Wexner Medical Center, Columbus, OH 43210, USA, [3]Texas Biomedical Research Institute, San Antonio, TX 78227, USA, [4]Department of Medicine, Columbia University Medical Center, NY, NY 10032, USA and [5]Department of Genetics, The University of Alabama at Birmingham, Birmingham, AL 35233, USA

Received September 29, 2021; Revised June 26, 2022; Editorial Decision July 10, 2022; Accepted July 20, 2022

ABSTRACT

FACT (FAcilitates Chromatin Transcription) is a heterodimeric protein complex composed of SUPT16H and SSRP1, and a histone chaperone participating in chromatin remodeling during gene transcription. FACT complex is profoundly regulated, and contributes to both gene activation and suppression. Here we reported that SUPT16H, a subunit of FACT, is acetylated in both epithelial and natural killer (NK) cells. The histone acetyltransferase TIP60 contributes to the acetylation of SUPT16H middle domain (MD) at lysine 674 (K674). Such acetylation of SUPT16H is recognized by bromodomain protein BRD4, which promotes protein stability of SUPT16H in both epithelial and NK cells. We further demonstrated that SUPT16H-BRD4 associates with histone modification enzymes (HDAC1, EZH2), and further regulates their activation status and/or promoter association as well as affects the relevant histone marks (H3ac, H3K9me3 and H3K27me3). BRD4 is known to profoundly regulate interferon (IFN) signaling, while such function of SUPT16H has never been explored. Surprisingly, our results revealed that SUPT16H genetic knockdown via RNAi or pharmacological inhibition by using its inhibitor, curaxin 137 (CBL0137), results in the induction of IFNs and interferon-stimulated genes (ISGs). Through this mechanism, depletion or inhibition of SUPT16H is shown to efficiently inhibit infection of multiple viruses, including Zika, influenza, and SARS-CoV-2. Furthermore, we demonstrated that depletion or inhibition of SUPT16H also causes the remarkable activation of IFN signaling in NK cells, which promotes the NK-mediated killing of virus-infected cells in a co-culture system using human primary NK cells. Overall, our studies unraveled the previously unappreciated role of FACT complex in coordinating with BRD4 and regulating IFN signaling in both epithelial and NK cells, and also proposed the novel application of the FACT inhibitor CBL0137 to treat viral infections.

INTRODUCTION

In eukaryotes, histone chaperones play a critical role in regulating gene expression by maintaining nucleosome assembly and genome stability (1). As one of key histone chaperones, the main function of FACT (FAcilitates Chromatin Transcription) complex is the deposition and reorganization of histone octamer in nucleosome (2–4). FACT participates in various processes, such as gene transcription, DNA replication and repair, and centromere activation (2,5,6). FACT is a heterodimer composed of two subunits, SUPT16H and SSRP1, which interact with each other as well as the nucleosome through specific domains. Beyond the common functions conveyed through FACT, both SUPT16H and SSRP1 possess their additional ones independent from each other (7,8).

Since the initial identification, FACT has been generally believed to facilitate gene transcription due to its control of nucleosome remodeling critical for the RNA polymerase II (Pol II) elongation (3). However, there is also increasing evidence supporting that FACT contributes to gene suppression through various mechanisms. For example, earlier studies from us revealed that FACT represses gene expression of HIV-1 proviruses integrated into host

*To whom correspondence should be addressed. Tel: +1 614 293 4543; Email: Jian.Zhu@osumc.edu
Correspondence may also be addressed to Netty G. Santoso. Tel: +1 614 685 0017; Email: Netty.Santoso@osumc.edu

genomes and promotes viral latency by interfering with the interaction between P-TEFb and viral Tat-LTR axis (9). Likewise, FACT has been recently reported to block lytic reactivation of latent Epstein-Barr virus (EBV) that tethers viral episomes with host genomes by supporting MYC expression in Burkitt lymphoma (BL) (10). FACT is known to inhibit the expression of cryptic genes, antisense transcripts, and subtelomeric genes (11,12). Retro-transposable elements and the associated cryptic promoters are also silenced by FACT (13). These data suggest that FACT plays a more profound role in regulating gene expression, while the underlying mechanisms contributing to such functions of FACT need more careful investigations.

One direction is to determine the impact of post-translational modifications (PTMs) on FACT's transcriptional activities. There has been a study showing that FACT undergoes K63-linked ubiquitination that affects its function during DNA replication (14). Beyond ubiquitination, other PTMs of FACT proteins are far from detailed characterizations. For example. impact of acetylation on FACT has never been deliberately examined, although several proteomic screenings have predicted that there are multiple acetylation sites of FACT subunit SUPT16H (15–18). However, there is currently no knowledge regarding whether acetylation of FACT proteins truly exists nor what is the functional contribution of FACT acetylation. Our studies started from the point to characterize the acetylation of FACT proteins, which led to the further findings that FACT subunit SUPT16H associates with BRD4 through its acetylation and contributes to silencing of interferon (IFN) signaling.

MATERIALS AND METHODS

Cells and plasmids

HEK293T, HeLa, Vero E6, TZM-bl and iSLK.BAC16 cells were maintained in Dulbecco's modified Eagle's medium (DMEM) (Sigma-Aldrich). A549 cells were maintained in Ham's F-12K (Kaighn's) medium (Gibco). Jurkat cells were maintained in RPMI 1640 medium (Gibco). K562 human myelogenous leukemia cells were maintained in Iscove's modified Dulbecco's medium (ATCC). All of above media were supplemented with 10% fetal bovine serum (FBS) (Gibco) and 1× penicillin–streptomycin solution (Corning). NK-92 (ATCC® CRL-2407™) human natural killer cells were cultured in Alpha Minimum Essential medium according to guideline from ATCC. iSLK.BAC16 cells were cultured in DMEM in the presence of 1 μg/ml puromycin, 250 μg/ml G418 and 1200 μg/ml hygromycin B. Telomerase-immortalized human microvascular endothelial (TIME) cells were maintained in Vascular Cell Basal Medium (ATCC) supplemented with Microvascular Endothelial Cell Growth Kit-VEGF (ATCC). Human PBMCs and primary NK cells were maintained in RPMI complete medium (15% FBS, 1× penicillin–streptomycin solution, 1× MEM non-essential amino acid solution, 1× sodium pyruvate and 20 mM HEPES) supplied with 30 units/ml of human recombinant IL-2 (rIL-2, Roche).

Four domains of SUPT16H, NTD, DD, MD and CTD, were cloned in pQCXIP (Clontech) with a N-terminal FLAG tag. Site-specific mutation of K674R, K661R, K786R, K904R was introduced in pQCXIP-FLAG-MD by using the QuikChange Lightning Site-Directed Mutagenesis Kit (Agilent Technologies) following the manufacturer's instructions. TIP60 shRNA (5'-TCG AAT TGT TTG GGC ACT GAT-3'), BRD4 shRNA (5'-CCA GGA CTT CAA CAC TAT GTT T-3') and firefly luciferase (FLuc) shRNA (5'-CAC AAA CGC TCT CAT CGA CAA G-3') were cloned in a pAPM lentiviral vector as previously described (19). SUPT16H MD wilt-type (WT) and K674R *att*B-PCR products were amplified from pQCXIP-FLAG-MD-WT and pQCXIP-FLAG-MD-K674R vectors, and cloned in pDONR223 and pET-DEST42 through Gateway BP and LR recombination reactions (Invitrogen), respectively. *cis*-reporting vectors of IFN activity, pISRE-Luc and pGAS-Luc, were purchased (Agilent Technologies). *Renilla* luciferase (RLuc) reporter vector pRL-TK was purchased (Promega). HDAC1 was cloned in pcDNA-DEST40 with a C-terminal V5 tag. pLX317-EZH2-V5 expression vector was acquired from Sigma-Aldrich.

Human peripheral blood mononuclear cells (PBMCs) and isolation of primary NK cells

Human PBMCs were isolated from healthy peripheral whole blood (STEMCELL Technologies) by using a gradient method with the Ficoll-Paque (GE Healthcare), and frozen for later use. Cryopreserved PBMCs were cultured in RPMI complete medium supplied with 30 units/ml of human recombinant IL-2 for three days, and the $CD56^{+}CD3^{-}$ NK cells were isolated by using the human NK cell isolation kit (Miltenyi Biotec) following the manufacturer's instructions.

Reagents and antibodies

DMSO was purchased from Fisher Scientific. JQ1 was purchased from Sigma-Aldrich. MG149, amlexanox, and GSK8612 were purchased from Selleck Chemicals. siRNAs targeting SUPT16H, BRD4, SSRP1, BRD2 and NT siRNA were purchased from Invitrogen. CBL0137 was provided by Cayman Chemical and purchased from Fisher Scientific. Recombinant TIP60 (KAT5) and recombinant BRD4 bromodomain 1 (BD1) were purchased from Active Motif. Recombinant BRD4 bromodomain 2 (BD2) was purchased from EpiCypher. TCEP-HCl was purchased from Thermo Scientific. Acetyl coenzyme A (acetyl-CoA) sodium salt was purchased from Sigma-Aldrich. Human IFNα (alpha 2a) and IFNγ were purchased from PBL Assay Science. BD GolgiStop™ protein transport inhibitor was purchased from BD Biosciences. Remdesivir was purchased from AOBIOUS.

The following antibodies were used in this study. Anti-acetyl lysine antibody was purchased from ImmuneChem. Anti-SUPT16H, anti-SSRP1, anti-BRD2, anti-IFI16, anti-MX1, anti-ISG15, anti-GAPDH and normal mouse IgG antibodies were purchased from Santa Cruz Biotechnology. The anti-BRD4 (targeting C-terminus of BRD4 1312–1362 aa) antibody was purchased from Bethyl Laboratories. The anti-BRD4 (targeting N-terminus of BRD4 154–

284 aa), anti-TIP60 (KAT5), anti-FLAG, anti-6× His, anti-V5, phospho-HDAC1 (ser421/423), normal rabbit IgG and Alexa Fluor 488 goat anti-mouse IgG antibodies were purchased from Invitrogen. Anti-K48Ub, anti-histone H3, anti-mouse HRP-linked and anti-rabbit HRP-linked antibodies were purchased from Cell Signaling Technology. Anti-HDAC1 antibody was purchased from Novus Biologicals. Anti-H3K9me3, anti-H3K27me3, anti-H3ac (pan-acetyl), anti-H4ac (pan-acetyl), anti-histone H4 and anti-EZH2 antibodies were purchased from Active Motif. PE/Cyanine7 anti-human CD107a (LAMP-1), PE anti-human IFNγ and anti-IL-6 antibodies were purchased from BioLegend. Anti-dsRNA (clone rJ2), anti-flavivirus group antigen antibody that probes ZIKV E protein and anti-SARS-CoV-1/2 nucleocapsid (N) protein 1C7C7 antibody were purchased from Sigma-Aldrich. Anti-influenza A virus nucleoprotein (NP) antibody was obtained from BEI Resources. Anti-IL-4, anti-IL-8 and FITC Mouse anti-rat IgG1 antibodies was purchased from BD Biosciences.

Proteins

pET-DEST42 vector containing SUPT16H MD WT or MD K674R domain (with C-terminal V5 and 6 × His tags) was transformed in BL21 (DE3) *E. coli* (Invitrogen) for protein expression and purification. Bacteria cells were incubated in LB media at 37°C until the optical density (OD) at 600 nm reached ∼0.6, followed by the protein induction with 0.1 mM IPTG for 16 h at 16°C. Bacteria cells were harvested, re-suspended in B-PER™ Bacterial Protein Extraction Reagent (Thermo Scientific) with 100 μg/ml lysozyme, 5 units/ml DNase I, and protease inhibitor cocktail (Thermo Scientific), and then incubated on ice for 30 min, followed by sonication. Cell debris were removed by centrifugation at 10 000 × g for 10 min at 4°C, and supernatant was loaded on the HisPur™ Ni-NTA Spin Columns (Thermo Scientific) to purify His-tagged proteins by following the manufacturer's instructions. Protein concentration was measured by the BCA assay.

Protein immunoblotting and immunoprecipitation

Protein immunoblotting and immunoprecipitation (IP) were performed as described previously (20). Briefly, total protein was extracted from cell lysates by using 1 × radioimmunoprecipitation assay (RIPA) buffer containing broad-spectrum protease inhibitors. Protein concentrations were measured by BCA assay, followed by electrophoresis and dry electro-transfer. The membrane was blocked with nonfat milk, and incubated with primary and HRP-conjugated secondary antibodies, followed by the incubation with ECL substrate. To determine acetylation, ubiquitination and other protein binders of the targeted proteins, cell lysates were incubated with the specific antibodies recognizing the targeted proteins or control IgG, followed by the incubation with protein A/G magnetic beads. Beads containing protein immunocomplexes were washed, eluted and subjected to protein immunoblotting. The intensity of protein bands was quantified by using the ImageJ software.

Chromatin immunoprecipitation (ChIP)

ChIP was performed as previously described (19). In brief, 1% paraformaldehyde (PFA) (Electron Microscopy Sciences) was used for cell cross-linking, followed by the addition of 125 mM glycine to quench the reaction. Cells were then re-suspended by CE buffer and centrifuged to pellet nuclei, which were further incubated with SDS lysis buffer and sonicated to generate DNA fragments. Nuclear lysates were diluted with CHIP dilution buffer and incubated with antibodies recognizing the targeted proteins or control mouse/rabbit IgG, followed by the incubation with protein A/G magnetic beads that were pre-blocked with 0.5 mg/ml BSA and 0.125 mg/ml herring sperm DNA (Invitrogen). The beads were subsequently washed with low-salt buffer, high-salt buffer, LiCl buffer and TE buffer, and the IPed protein-DNA complexes were eluted by elution buffer. To recover DNA samples, the elutes were treated with 0.2 M NaCl and incubated at 65°C for overnight, followed by the treatment of EDTA, Tris–HCl (pH 6.5), and proteinase K. DNA samples were extracted by phenol/chloroform/isoamyl alcohol (25:24:1). DNA pellets were re-suspended in nuclease-free water, which were used for qPCR analysis. Input (5%) was also included.

In vitro acetylation assay

V5–6× His-tagged SUPT16H MD WT or MD-K674R domain (2 μg) was mixed with the increasing amount of recombinant TIP60 protein (0, 100, 200 ng) in acetyltransferase reaction buffer (50 mM Tris–HCl [pH 8.0], 0.1 mM EDTA, 50 ng/μl BSA, 1 mM TCEP and 20 μM acetyl-CoA), and incubated for 2 h at room temperature (RT). Protein samples were denatured by 2× SDS buffer (Invitrogen), and proteins were analyzed by immunoblotting.

In vitro BD pull-down assay

Recombinant SUPT16H MD WT or K674R domain (4 μg) purified from *E. coli* was acetylated by TIP60 (400 ng). Proteins were then mixed with the anti-V5 antibody in the binding buffer (50 mM Tris [pH7.5], 150 mM NaCl, 0.1% NP-40) for 2 h with rotation at RT, followed by the further incubation with protein A/G magnetic beads (pre-washed with binding buffer) for 1 h with rotation at RT. Beads were collected by a magnetic separator, and washed for four times with binding buffer. The purified, acetylated MD WT or K674R domain on beads was further incubated with or without 2 μg recombinant BRD4 BD1 or BD2 domain in binding buffer for overnight with rotation at 4°C. The beads were then washed with binding buffer for four times, and protein samples were analyzed by immunoblotting.

Luciferase reporter assay

HEK293T cells were reversely transfected with gene-specific siRNAs using Lipofectamine™ RNAiMAX Transfection Reagent (Invitrogen). At 72 h post-transfection, cells were further transfected with pISRE-Luc or pGAS-Luc vector along with pRL-TK by using the TurboFect™ Transfection Reagent (Thermo Scientific) for 24 h. Cells were then treated with stimulators (IFNα, IFNγ) for 24

h, followed by the measurement of firefly/*Renilla* luminescence using the Dual-Glo® luciferase assay system (Promega). Luminescence was measured by the Cytation 5 multimode reader (BioTek), and the relative luciferase unit (RLU) was calculated. To determine the HIV-1 LTR promoter activity, TZM-bl cells harboring LTR-luciferase reporter were reversely transfected with siRNAs for 72 h, followed by TNFα treatment for 24 h. Luminescence was measured and normalized to total proteins quantified by BCA assay.

Cell viability assay

ATP-based CellTiter-Glo Luminescent Cell Viability Assay (Promega) was used to measure drug cytotoxicity or cell killing following the manufacturer's instructions. Luminescence was measured by the Cytation 5 multimode reader (BioTek).

Propagation and infection of KSHV

KSHV BAC16 was propagated as previously described with slight modifications (21,22). In brief, iSLK.BAC16 cells were treated with 2 μg/ml doxycycline together with 1 mM sodium butyrate (NaB) for 24 h to reactivate KSHV. Cells were then kept in fresh medium containing 2 μg/ml doxycycline that was supplemented every 2 days. At day 5 post of reactivation, supernatants were collected, centrifuged (400 × g) for 10 min to remove cell debris, and filtered through the 0.45 μm filter. KSHV BAC16 stock was titrated in HEK293T cells through the serial dilution. Pre-seeded cells were infected with KSHV BAC16 via spinoculation (2500 rpm) for 2 h at 37°C.

Immunofluorescence assay (IFA)

IFA for measurement of intracellular proteins followed by flow cytometry analysis was performed as previously described (20). Briefly, 1×10^6 cells were washed with 1× D-PBS and fixed with 4% PFA. 1× Perm/Wash buffer (BD Biosciences) containing saponin was used for cell permeabilization, followed by the incubation with primary antibodies and fluorophore-conjugated secondary antibodies. Cell samples were washed and re-suspended with staining buffer, which was subjected to flow cytometry analysis using the BD Accuri C6 Plus with the corresponding optical filters. Mean fluorescence intensity (MFI) was determined by using the FlowJo V10 software.

IFA for measurement of intracellular proteins using microscopy was also performed. HeLa or A549 cells were seeded at the density of 8000 cells/well on 96-well culture plates. At 24 h post of seeding, cells were treated with CBL0137 (200 nM), or IFNα (1×10^4 units/ml) and IFNγ (100 ng/ml) for 24 h, followed by the infection of ZIKV (Fortaleza strain, MOI = 0.5) for 48 h or influenza A virus (A/WSN/1933 [H1N1] strain, MOI = 0.5) for 24 h. HeLa cells were also reversely transfected with SUPT16H, SSRP1 or NT siRNAs for 48 h, followed by the infection of ZIKV (MOI = 0.5). For measurement of dsRNA, pre-seeded HeLa cells were either treated with CBL0137 (100, 200 and 500 nM), or infected with ZIKV (MOI = 0.2) for 24 h. Cells were fixed with 4% paraformaldehyde at RT for 10 min and permeabilized with 0.2% Triton X-100 at RT for 15 min, followed by blocking with 1× D-PBS containing 5% FBS for 1 h at RT. Cells were then incubated with primary antibodies in 1× D-PBS containing 2.5% FBS for overnight at 4°C, and Alexa Fluor 488-conjugated secondary antibodies for 1 h at RT. Nuclei were stained with Hoechst 33342 (Thermo Scientific) for 10 min at RT. Cells were imaged by using the Cytation 5 multi-mode reader. Percentages of virus-infected cells was quantified by using the Gen5 Image+ software (BioTek).

Quantitative reverse transcription PCR (RT-qPCR)

Total RNAs were extracted from cells by using the NucleoSpin RNA isolation kit (MACHEREY-NAGEL). Eluted RNA samples were reverse transcribed by using the iScript cDNA Synthesis Kit (Bio-Rad). qPCR was performed by using the iTaq Universal SYBR Green Supermix (Bio-Rad) on a CFX Connect Real-Time PCR System (Bio-Rad). The primers used for qPCR were listed in Supplementary Table S1.

RNA-seq assay

NK-92 cells were treated with CBL0137 (500 nM) or DMSO for 24 h. RNA samples from four independent repeats were extracted by using the NucleoSpin RNA isolation kit following manufacturer's manual. RNA samples were submitted to GENEWIZ (South Plainfield, NJ 07080). RNA samples that passed quality control were subjected to rRNA removal through polyA selection, followed by the library preparation. Sequencing was carried out on an Illumina HiSeq platform with the configuration of 2 × 150 bp (paired end), and >20 million reads per sample were achieved. Differential expression of genes was analyzed by DESeq2 (23). R packages, pheatmap and clusterProfiler, were used for heatmap construction and pathway analysis, respectively. Published RNA-seq data (GEO accession: GSE126442) (24) were analyzed by using the similar methods.

Analysis of ChIP-seq datasets

ChIP-seq analysis was performed by following the modified ChiLin pipeline (25). Briefly, ChIP-seq data was mapped to mm10 using bowtie2 (version 2.3.4.3). Unmapped, mate unmapped, not primary alignment, multi-mapped, low mapping quality (MAPQ < 30), duplicate reads, and PCR duplicates were removed. Peaks were called by MACS2 (version 2.2.4), with parameters -B -q 0.01 –keep-dup 1 –nomodel -g mm –f BAM/BAMPE. For visualization, bedGraph files were generated by MACS2 bdgcmp from the pile-up, and then converted to bigwig format with bedGraphToBigWig. Overlapping between SUPT16H and BRD4 ChIP-seq peaks was determined by using the BedTools intersect command if at least 1 bp of each peak overlaps (26–28).

NK cell cytotoxicity and cell killing assays

NK cell-mediated cytotoxicity was assessed by measuring the expression of degranulation marker CD107a and the

production of IFNγ as previously described with slight modifications (29). In brief, K562 target cells were pre-stained with the CellTrace™ CFSE Cell Proliferation Kit (Invitrogen) according to the manufacturer's protocols. 1×10^6 NK-92 cells were co-cultured with the same number of K562 cells (1:1 of effector: target [E:T] ratio) for 4 h. PE/Cy7-CD107a antibody (Biolegend) was added. Cells were then treated with GolgiStop (BD Biosciences) for 1 h, and washed with 1× D-PBS. After cell fixation and permeabilization, intracellular IFNγ was stained by PE-IFNγ antibody (Biolegend). Fluorescent signal of CD107a or IFNγ in NK-92 cells (CFSE-negative) was determined by flow cytometry analysis. MFI was calculated by using the FlowJo V10 software.

NK cell-mediated killing of virus-infected cells was also performed. HeLa cells were seeded at 24 h prior to viral infection with 8000 cells/well on 96-well plates. Cells were then infected with ZIKV (MOI = 2) for 48 h. NK-92 cells were reversely transfected with SUPT16H or NT siRNAs for 72 h prior to the cell co-culture. NK-92 or primary NK cells were also treated with CBL0137 (500 nM) for 48 h before the co-culture, and CBL0137 was washed away at 24 h post of treatment. NK-92 or primary NK cells were then co-cultured with HeLa cells (2:1 or 1:5 of effector: target [E:T] ratio, respectively) for 6 h. NK cells were removed. HeLa cells were washed twice with DMEM. Survival of HeLa cells was determined by using the ATP-based CellTiter-Glo Luminescent Cell Viability Assay. Percentage of NK cell-mediated killing was calculated as below:

$$\%\,\text{Killing of HeLa cells} = 100 - \frac{\%\,\text{Cell viability of HeLa transfected with SUPT16H siRNAs (or treated with CBL0137)}}{\%\,\text{Cell viability of HeLa transfected with NT siRNAs (or treated with DMSO)}} \times 100$$

Plaque reduction microneutralization (PRMNT) assay

PRMNT assay was performed to evaluate the antiviral activity of drugs against SARS-CoV-2 as previously described (30). In brief, Vero E6 cells were seeded on 96-well plates with 1×10^4 cells/well at 24 h prior to viral infection. Cells were infected (100–200 PFU/well) with SARS-CoV-2 (USA-WA1/2020 strain) at 37°C for 1 h in the CO_2 incubator. Viral inoculum was removed, and 2-fold serial dilutions of the drugs were added. At 24 h post-treatment, cells were fixed with 10% formalin solution and permeabilized with 0.5% Triton X-100, followed by blocking with 2.5% BSA in PBS. Cells were then incubated with primary antibody targeting SARS-CoV-1/2 N (1C7C7) and biotinylated secondary antibody. Cells labeled with biotin were detected using the VECTASTAIN® ABC-HRP Kit, Peroxidase (Mouse IgG) (Vector Laboratories) following the manufacturer's instructions. Viral plaques were counted on the CTL ImmunoSpot plate reader. Infections with SARS-CoV-2 was carried out at a BSL3 laboratory. Percentage of viral infection was calculated as below:

$$\%\,\text{Viral infection} = \frac{\text{Number of plaques with drug treatment} - \text{Number of plaques with ''No virus''}}{\text{Number of plaques with ''No drug''} - \text{Number of plaques with ''No virus''}} \times 100$$

Statistical analysis

Results were acquired from at least three independent repeats, and analyzed by using either the unpaired, two-tailed Student's *t* test or the one-way/two-way analysis of variance (ANOVA). A *P* value <0.05 was considered as statistically significant ($*P < 0.05$, $**P < 0.01$, $***P < 0.001$, $****P < 0.0001$). The Pearson's *r* was used for the correlation analysis. Results were presented as either means ± standard deviation (SD) or means ± standard error of the mean (SEM), and graphed by using the GraphPad Prism 9.0 software.

RESULTS

SUPT16H is acetylated by TIP60 and interacts with BRD4

To determine the acetylation of FACT proteins, we performed protein immunoprecipitation (IP) using an anti-acetyl lysine antibody in different cell lines, including HEK293T, Jurkat, HeLa and NK-92 cells, followed by immunoblotting of FACT proteins. Acetylation of SUPT16H, but not SSRP1, can be readily detected in all tested cell lines (Figure 1A). We further spent effort searching for the acetyltransferase(s) that contributes to SUPT16H acetylation. Previous studies showed that in yeast, the FACT complex subunit Spt16 interacts with Sas3, a MYST-family histone acetyltransferase (HAT) that shares the homology with human TIP60 across multiple regions (31). TIP60 also has a BRD4-dependent function to suppress endogenous retroviruses (ERVs), indicating that TIP60 and BRD4 may work coordinately to silence gene expression (32). Based on the above knowledge, we hypothesized that TIP60, a well-studied HAT catalyzing acetylation of various histone and nonhistone proteins, may participate in the acetylation of SUPT16H. We showed that TIP60 interacts with SUPT16H (Figure 1B) and that its knockdown by shRNA significantly reduces SUPT16H acetylation (Figure 1C and D). Consistently, treatment of a TIP60-specific inhibitor MG149 also led to the reduction of SUPT16H acetylation without obvious cytotoxicity (Figure 1E, Supplementary Figure S1A). Protein acetylation can be recognized by certain readers that further recruit downstream executers to fulfill regulatory functions (33). We found that SUPT16H interacts with BRD4, a key acetylation reader containing two bromodomains, whereas SSRP1 has no such interaction with BRD4 (Figure 1F, Supplementary Figure S2A). Beside BRD4, we found that BRD2 does not interact with SUPT16H (Figure 1G), even though BRD2 is also a bromodomain-containing protein that closely relates with BRD4 evolutionarily (34). These results also supported the earlier findings that the BET (bromodomain and extra terminal domain) family proteins (BRD2, BRD3, BRD4 and BRDT) possess the different patterns of bromodomain-dependent interactions with the acetylated proteins (35–37). Furthermore, it has been reported that BRD4 protein has long and short isoforms (38), BRD4L (~190 kDa) and BRD4S (~130 kDa). The BRD4 antibody used for BRD4–SUPT16H protein interaction studies (Figure 1F, and G) recognizes the C-terminus of BRD4 protein (1312–1362 aa) and thus shall technically only identify BRD4L but not BRD4S. We no-

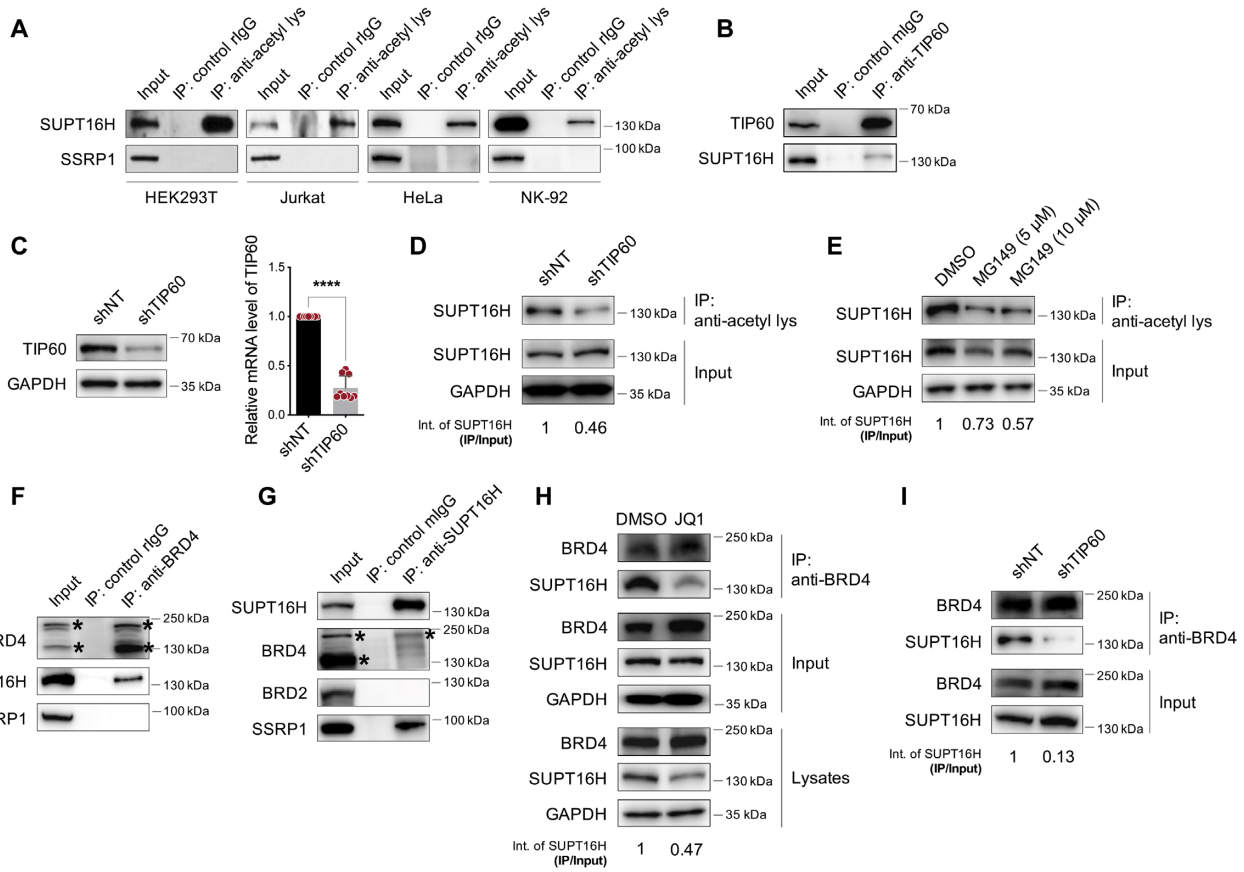

Figure 1. SUPT16H acetylation requires TIP60 and is recognized by BRD4. (**A**) Lysates of HEK293T, Jurkat, HeLa and NK-92 cells were incubated with an acetyl-lysine antibody or normal rabbit IgG (rIgG). Immunoprecipitated protein samples were analyzed by protein immunoblotting using SUPT16H or SSRP1 antibodies. (**B**) Lysates of HEK293T cells were incubated with a TIP60 antibody or normal mouse IgG (mIgG). Immunoprecipitated protein samples were analyzed by protein immunoblotting using SUPT16H or TIP60 antibodies. (**C**) HEK293T cells stably expressing TIP60 or non-targeting (NT) shRNA were subjected to protein immunoblotting and RT-qPCR analyses of TIP60 expression. RT-qPCR results were calculated from three independent experiments (**** $P < 0.0001$, Student's *t*-test). (**D**) Lysates of HEK293T cells in (**C**) were incubated with an acetyl-lysine antibody. Immunoprecipitated protein samples were analyzed by protein immunoblotting using a SUPT16H antibody. (**E**) Lysates of HEK293T cells treated with a TIP60-specific inhibitor MG149 were incubated with an acetyl-lysine antibody. Immunoprecipitated protein samples were analyzed by protein immunoblotting using a SUPT16H antibody. (**F**) Lysates of HEK293T cells were incubated with a BRD4 antibody (C-terminus) or rIgG. Immunoprecipitated protein samples were analyzed by protein immunoblotting using SUPT16H, SSRP1, or BRD4 (C-terminus) antibodies. (**G**) Lysates of HEK293T cells were incubated with a SUPT16H antibody or mIgG. Immunoprecipitated protein samples were analyzed by protein immunoblotting using BRD4 (C-terminus), BRD2, SSRP1 or SUPT16H antibodies. The higher band of BRD4 in (**F**) and (**G**) labeled with the asterisk was BRD4L, while the lower one was its degraded product. (**H**) Lysates of HEK293T cells treated with a BETi JQ1 (1 μM) were adjusted to assure the same input of SUPT16H, and incubated with a BRD4 antibody (C-terminus). Immunoprecipitated protein samples were analyzed by protein immunoblotting using SUPT16H or BRD4 (C-terminus) antibodies. (**I**) Lysates of HEK293T cells in (**C**) were incubated with a BRD4 antibody (C-terminus). Immunoprecipitated protein samples were analyzed by protein immunoblotting using SUPT16H or BRD4 (C-terminus) antibodies. (Int: intensity)

ticed there are two bands between 130 and 250 kDa, and we expected that the higher band is BRD4L while the lower one is its degraded product. Alternatively, we confirmed BRD4-SUPT16H protein interaction by using another BRD4 antibody that recognizes the N-terminus of BRD4 protein (154–284 aa) and thus shall technically identify both BRD4L and BRD4S. We also noticed there are two bands between 130 and 250 kDa, and we expected that the higher band is BRD4L while the lower one is BRD4S (Supplementary Figure S3A). In this case, we observed that only BRD4L but not BRD4S interacts with SUPT16H. Treatment of a bromodomain and extra-terminal motif inhibitor (BETi) JQ1 led to the drastic reduction of SUPT16H and BRD4 interaction (Figure 1H), reassuring that BRD4 interaction with SUTP16H is through its acetyl lysine-binding capacity. Furthermore, knockdown of TIP60 also greatly decreased the SUPT16H and BRD4 interaction (Figure 1I). Overall, these results indicated that SUPT16H is acetylated by TIP60 and that SUPT16H acetylation mediates protein interaction of SUPT16H and BRD4.

SUPT16H middle domain (MD) is acetylated at K674 that mediates BRD4 interaction

To further characterized SUPT16H acetylation, four domains of SUPT16H, including N-terminal domain (NTD), dimerization domain (DD), middle domain (MD), and C-terminal domain (CTD), were cloned in pQCXIP vector and expressed with an N-terminal FLAG tag (Figure 2A). These vectors were transfected in HEK293T cells, which were subjected to the reciprocal protein IP assays. Both DD and MD domains from acetylation pull-down were detected

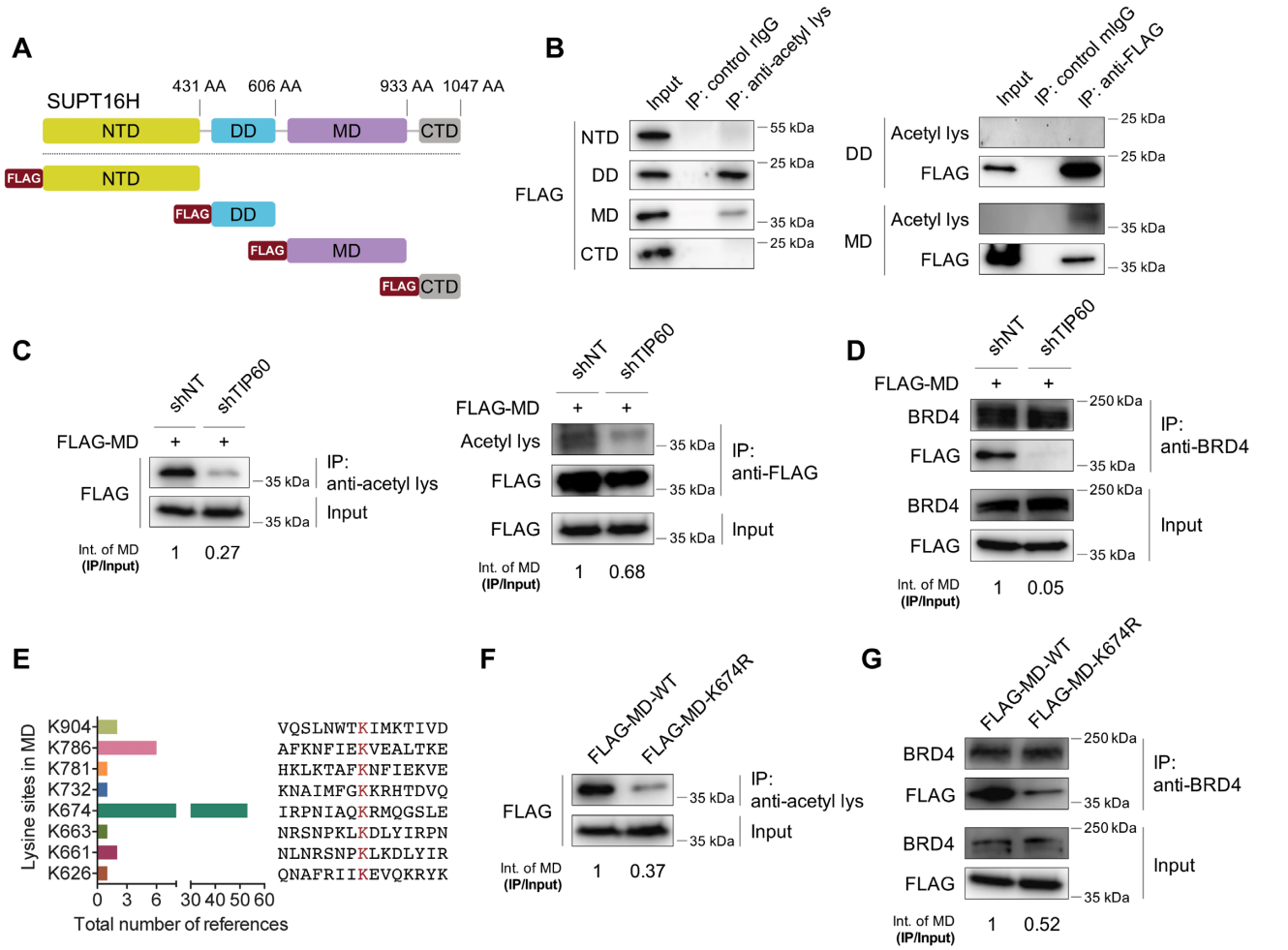

Figure 2. SUPT16H is acetylated at K674 of the middle domain (MD). (**A**) Schematic illustration of defined domains of SUPT16H protein. NTD: N-terminal domain; DD: dimerization domain; MD: middle domain; CTD: C-terminal domain. (**B**) Lysates of HEK293T cells transfected with the vector expressing indicated FLAG-tagged protein domains of SUPT16H were incubated with an acetyl-lysine or FLAG antibody, and immunoprecipitated protein samples were analyzed by protein immunoblotting using FLAG or acetyl-lysine antibodies, respectively. (**C**) HEK293T cells stably expressing TIP60 or NT shRNA were transfected with the vector expressing FLAG-tagged MD of SUPT16H. Cell lysates were incubated with acetyl-lysine or FLAG antibodies, and immunoprecipitated protein samples were analyzed by protein immunoblotting using FLAG or acetyl-lysine antibodies, respectively. (**D**) Lysates of HEK293T cells in (**C**) were incubated with a BRD4 antibody (C-terminus). Immunoprecipitated protein samples were analyzed by protein immunoblotting using FLAG or BRD4 (C-terminus) antibodies. (**E**) Prediction of acetylated lysine sites in the MD of SUPT16H by PhosphoSitePlus®. Lysine site K674 has the highest likelihood to be acetylated. (**F**) Lysates of HEK293T cells transfected with FLAG-tagged, wild-type (WT) or K674R MD of SUPT16H, were incubated with an acetyl-lysine antibody. Immunoprecipitated protein samples were analyzed by protein immunoblotting using a FLAG antibody. (**G**) Lysates of HEK293T cells in (**F**) were incubated with a BRD4 antibody (C-terminus). Immunoprecipitated protein samples were analyzed by protein immunoblotting using FLAG or BRD4 (C-terminus) antibodies.

by FLAG immunoblotting, but only MD domain from FLAG pull-down was detected by acetylation immunoblotting (Figure 2B). These results suggested that only MD domain of SUPT16H is directly acetylated while DD domain likely binds to other acetylated proteins. We further confirmed the functional relevance of TIP60 and BRD4 using the SUPT16H MD domain. TIP60 knockdown significantly reduced the acetylation of MD domain in the reciprocal protein IP assays (Figure 2C). BRD4 interacted with MD domain, which was abolished due to TIP60 knockdown (Figure 2D). We next mapped the acetylation site of SUPT16H MD domain. Earlier proteomic analyses predicted that K674 of MD domain has the highest likelihood of acetylation (16,17) (Figure 2E). We mutated the lysine to arginine at 674 (K674R) of MD domain, which led to the reduction of MD acetylation (Figure 2F) as well as MD interaction with BRD4 (Figure 2G). In addition to K674, we also prepared K to R mutation for three other predicted lysine sites, K661, K786 and K904 (Figure 2E). There was little change of MD acetylation due to such mutation (Supplementary Figure S3B), indicating that K674 is the dominant site of acetylation in SUPT16H MD. To further confirm TIP60-mediated acetylation at K674, we purified wild-type (WT) and K674R recombinant MD protein domains for an *in vitro* TIP60 acetylation assay. TIP60 only acetylated WT but not K674R MD in a dose-dependent manner (Supplementary Figure S3C). Furthermore, these TIP60-acetylated WT and K674R MD domains were further subjected to an *in vitro* bromodomain (BD) pull-down assay. Results showed that WT MD domain preferentially inter-

acts with BRD4 BD1 versus BD2, while K674R MD has the significantly less interaction with either BD1 or BD2 in contrast to WT MD (Supplementary Figure S3D). Indeed, it was reported that BRD4 BD1 and BD2 have the distinct binding specificities (35). Above all, our results verified that MD domain of SUPT16H is acetylated at K674 by TIP60 and recognized by BRD4.

BRD4 interaction enhances protein stability of SUPT16H

We next addressed what is the functional impact of SUPT16H acetylation. We noticed that treatment with JQ1 leads to the drastic reduction of SUPT16H and BRD4 interaction (Figure 1H), and causes the notable reduction of SUPT16H protein in all tested cell lines (Figure 3A). Consistently, treatment of an alternative BETi UMB-136 (39) with the different chemical structure as JQ1 also rendered the similar effect on SUPT16H protein (Figure 3B). To reassure it is due to BRD4, we determined the effect of BRD4 knockdown on both mRNA and protein levels of SUPT16H. Our results showed that BRD4 knockdown by its shRNA (Supplementary Figure S4A) has no effect on SUPT16H mRNA but leads to the dramatic decrease of SUPT16H protein (Figure 3C, D). BRD4 knockdown by its siRNAs (Supplementary Figure S4B) yielded the similar results (Figure 3E and F). In comparison, BRD2 knockdown by its siRNAs showed no effect on the protein level of SUPT16H (Supplementary Figure S4C). Indeed, the ubiquitination-mediated proteolysis plays an important role in regulating the functions of FACT subunit SUPT16H (14,40). We further confirmed that treatment of JQ1 strongly increases the K48-linked ubiquitination of SUPT16H, which explains the JQ1-induced reduction of SUPT16H protein likely through the ubiquitination-mediated protein degradation (Figure 3G). Intriguingly, depletion of SSRP1 by its siRNAs led to the significant reduction of SUPT16H protein (Supplementary Figure S2B), which is consistent with early reports (13,41). Taken together, our results delineated that BRD4 binding to SUTP16H prevents K48-linked ubiquitination and protein degradation of SUPT16H.

SUPT16H–BRD4 binds to epigenetic silencing enzymes leading to gene suppression

Our earlier studies demonstrated that both SUPT16H and BRD4 contribute to the silencing of integrated HIV-1 proviruses (9,42), indicating that SUPT16H and BRD4 also possess gene suppression functions, which has not been characterized in details comparing to their well-studied roles in transcriptional activation. We confirmed that knockdown of SUPT16H or BRD4 by their specific siRNAs increases HIV-1 LTR promoter driven gene expression (Supplementary Figure S4D, E). Since we identified that BRD4 binds to SUPT16H, we speculated that SUPT16H-BRD4 renders gene suppression functions coordinately.

It was reported that SUPT16H interacts with SIN3-HDAC1 complex, which is identified from a high-sensitive affinity chromatography coupled with mass spectrometry proteomic analysis (43). In addition, it was known that SUPT16H binds to CENP-T/W complex that also interacts with EZH2 to promote gene silencing (44). HDAC1 and EZH2 are two key epigenetic silencing enzymes acting through modulation of histone deacetylation and methylation, respectively. Therefore, we hypothesized that SUPT16H–BRD4 associates with these epigenetic silencing enzymes contributing to gene suppression. As the supportive evidence, an earlier proteomic study predicted that EZH2 protein is a potential binding partner of SUPT16H (45). Our own results confirmed that SUPT16H–BRD4 indeed interacts with HDAC1 and EZH2 by a series of protein IP assays. HEK293T cells were transfected with V5-tagged HDAC1 or EZH2, and the V5 IP led to the pull-down of endogenous SUPT16H and BRD4 (Figure 4A, B). Endogenous HDAC1 or EZH2 were IPed using their specific antibodies, which also pulled down endogenous SUPT16H and BRD4 (Figure 4C and D). In the reciprocal IP of endogenous SUPT16H, EZH2, HDAC1, and BRD4 were all pulled down as well (Figures 4E, and 1G, Supplementary Figure S3A). We further determined whether such protein interaction of SUPT16H–BRD4–HDAC1 affects the activation status of HDAC1. Intriguingly, treatment of BRD4 inhibitors (JQ1, UMB-136, Figure 4F and G) or FACT inhibitor (curaxin CBL0137, Figure 4H) consistently led to the drastic decrease of HDAC1 phosphorylation at serine 421 and 423 (ser421/423) that is required for activation of its deacetylation activity (46). Similar results were obtained in the scenario of BRD4 (Figure 4I and J) or SUPT16H (Figure 4K and L) knockdown. Supportive evidence is that treatment of CBL0137 indeed significantly increases the cellular level of acetylated histone H3 (H3ac, Figure 4M) but not acetylated histone H4 (H4ac, Supplementary Figure S5A), indicating that SUPT16H preferentially impacts HDAC1-mediated deacetylation of H3 versus H4. As the next step, we determined the impact of SUPT16H–BRD4 on promoter-associated protein level of HDAC1, phosphorylated HDAC1 (ser421/423), as well as EZH2. We found that knockdown of SUPT16H or BRD4 indeed significantly reduces their promoter association at IFI44L and MX2 genes (Figure 4N and O). Such decrease of EZH2 at promoter regions correlated with another finding that treatment of CBL0137 also significantly decreases the cellular level of histone methylation marks, H3K27me3 and H3K9me3 as the direct (47) and indirect targets of EZH2 (48,49) (Supplementary Figure S5B). Overall, these results suggested that one potential new mechanism for SUPT16H–BRD4 to exert gene suppression functions is to interact with epigenetic silencing enzymes (HDAC1 and EZH2) and thus regulate their activation status and/or chromatin association.

We further confirmed the gene silencing functions of BRD4 and SUPT16H by using human endogenous retroviruses (HERVs) that closely resemble HIV-1 proviruses as examples. Knockdown of BRD4 or SUPT16H by their specific siRNAs indeed upregulated the expression of several HERVs in HEK293T cells (Supplementary Figure S6A, C). Treatment of CBL0137 also caused the induction of HERVs gene expression in NK-92 cells (Supplementary Figure S6E). Additionally, we also tested the role of SUPT16H-BRD4 in silencing certain non-coding repetitive elements, including human alpha satellite (SATα), pericentromeric

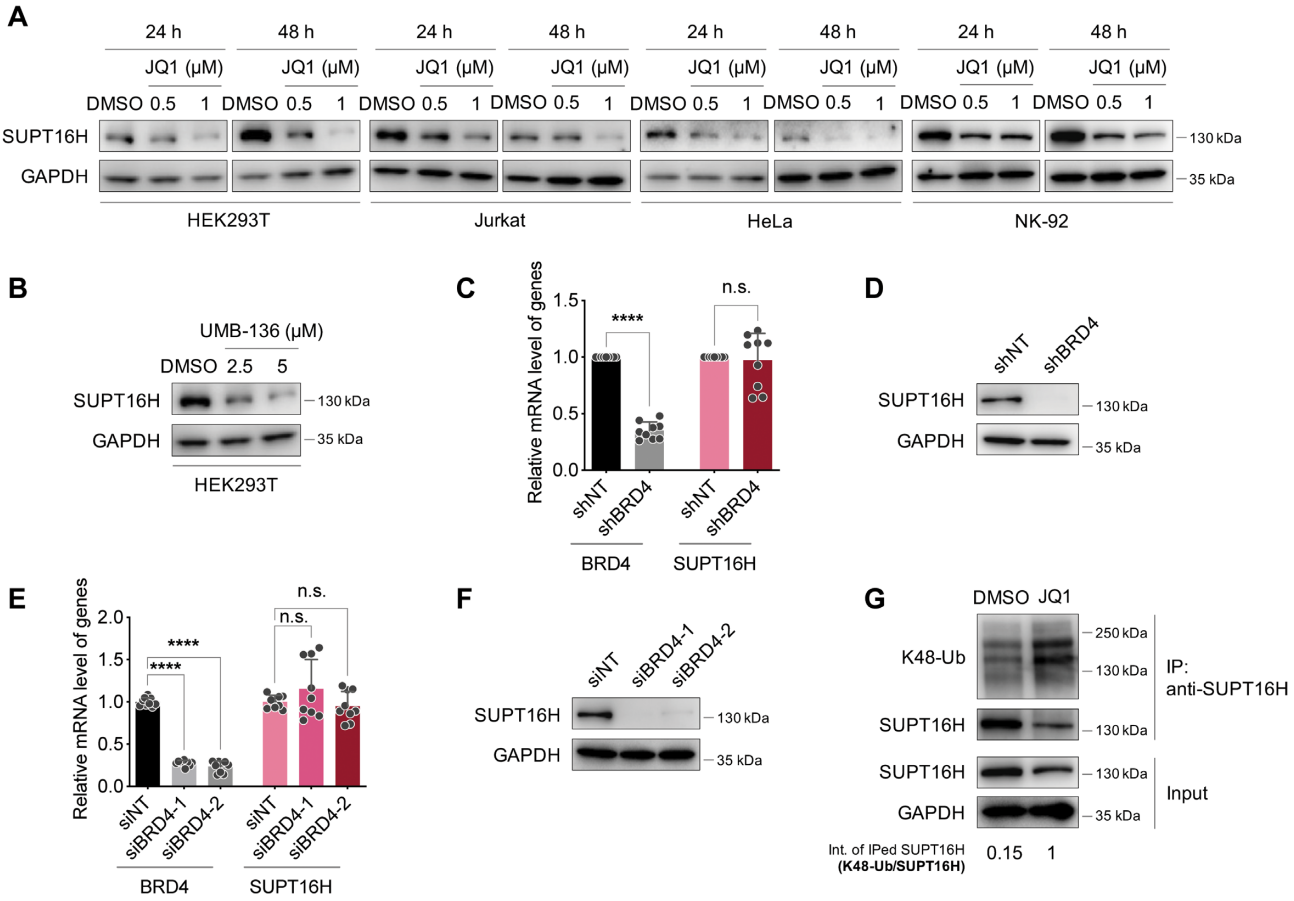

Figure 3. SUPT16H-BRD4 interaction prevents SUPT16H from protein degradation. (**A**) HEK293T, Jurkat, HeLa and NK-92 cells treated with JQ1 were subjected to protein immunoblotting analysis using a SUPT16H antibody. (**B**) The similar analysis as in (A) was performed for HEK293T cells treated with UMB-136 for 48 h. (**C, D**) HEK293T cells stably expressing BRD4 or NT shRNA were subjected to mRNA RT-qPCR analysis of BRD4 or SUPT16 expression (**C**) or protein immunoblotting analysis using a SUPT16H antibody (D). (**E, F**) The similar analysis as in (C, D) was performed for HEK293T cells transfected with BRD4 or NT siRNAs. Results were calculated from three independent experiments (**** $P < 0.0001$, Student's t test for C, one-way ANOVA for E). (**G**) Lysates of HEK293T cells treated with JQ1 (1 μM) were incubated with a SUPT16H antibody. Immunoprecipitated protein samples were analyzed by protein immunoblotting using K48-ubquitin or SUPT16H antibodies.

SST1 and subtelomeric D4Z4. Results showed that depletion of SUPT16H or BRD4, or CBL0137 treatment, moderately induces their expression (Supplementary Figure S6B, D, F).

SUPT16H–BRD4 controls the induction of IFN signaling via epigenetic suppression

Beyond HERVs and non-coding repetitive elements, we aimed to identify other cellular genes or gene sets subjected to SUPT16H–BRD4 mediated gene silencing. BRD4 has been implicated in regulation of gene expression in IFN signaling, and JQ1 has been reported to induce IFN signaling (50,51). However, such events have not been explored for SUPT16H. Reanalysis of previously published ChIP-seq datasets of mouse SUPT16H and BRD4 in the same cell type (52,53) supported that SUPT16H and BRD4 coordinately regulate the expression of immune genes (Supplementary Figure S5C, D), although these ChIP-seq datasets were generated by two different studies. Specifically, there are 466 (all regions) and 293 (promoter regions) peaks that overlap between SUPT16H and BRD4, corresponding to 399 and 267 all genes that include 128 and 84 immune genes, respectively. Furthermore, we found that knockdown of BRD4 or SUPT16H by their specific siRNAs indeed increases the expression of IFNβ and ISG15 in HEK293T cells (Figure 5A, and B). Additionally, knockdown or pharmacological inhibition of SUPT16H also caused the upregulation of interleukin (IL) genes, including IL-4, 6, 8, in both HEK293T (Figure 5C) and NK-92 cells (Supplementary Figure S1B, 5D, E). These results reassured that SUPT16H also participates in the modulation of IFN signaling, which was further investigated. We showed that knockdown of SUPT16H enhances the luciferase expression driven by interferon-sensitive responsive element (ISRE) and interferon-gamma activated site (GAS), which mediate the activation of type I and II IFN responses, IFNα/β and IFNγ, respectively (Figure 5F, G). Similarly, knockdown of SSRP1 also enhanced ISRE/GAS-driven luciferase expression (Supplementary Figure S2C, D), likely due to its impact on SUPT16H (Supplementary Figure S2B). Furthermore, treatment of CBL0137 led to the dramatic increase of H3ac but decrease of H3K9me3, H3K27me3 near promoter regions of ISGs and ILs in

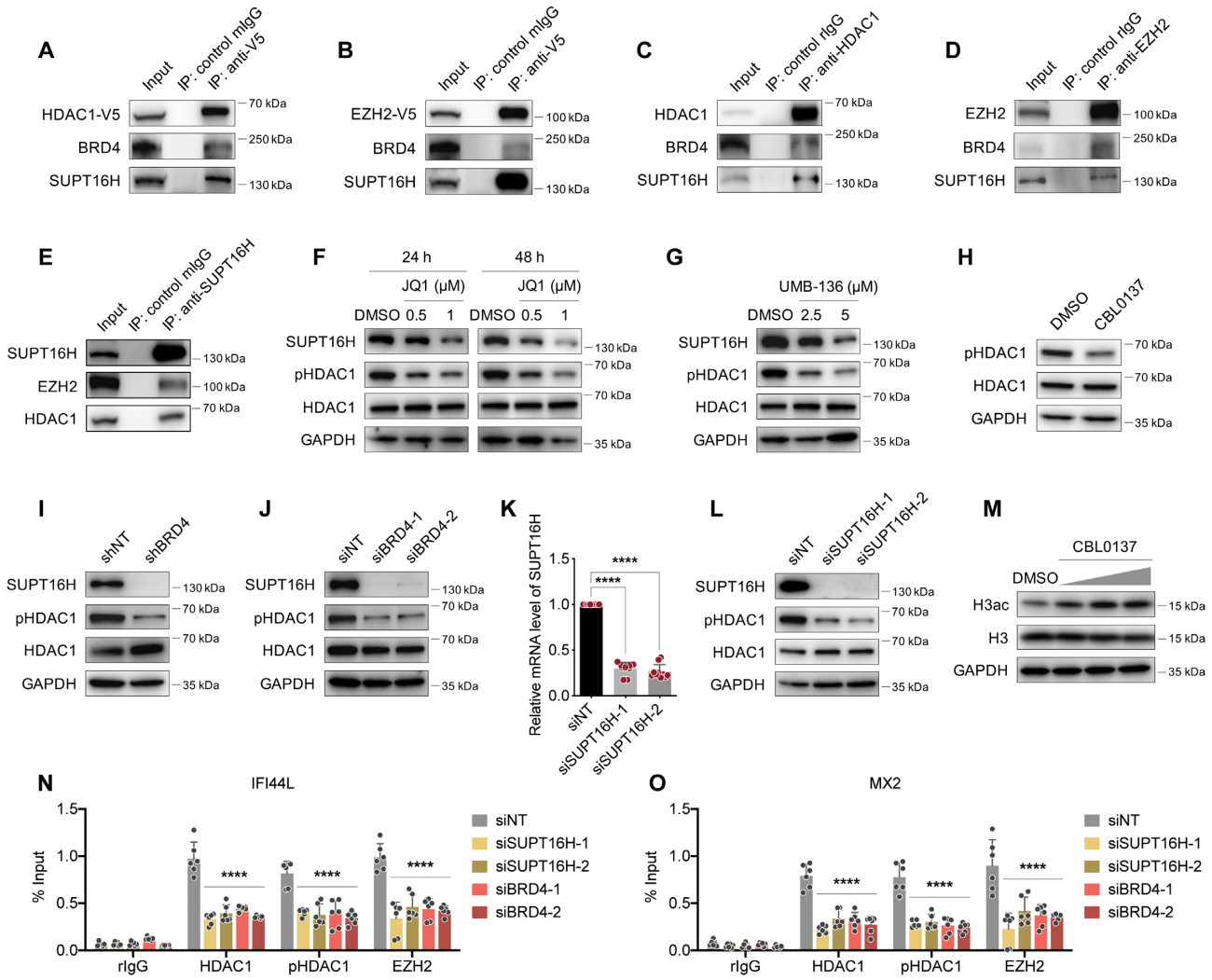

Figure 4. SUPT16H-BRD4 associates with HDAC1 and EZH2 contributing to gene silencing. (A, B) Lysates of HEK293T cells transfected with the vector expressing V5-tagged HDAC1 (**A**) or EZH2 (**B**) were incubated with a V5 antibody or mIgG. Immunoprecipitated protein samples were analyzed by protein immunoblotting using SUPT16H, BRD4 (C-terminus), or V5 antibodies. (C–E) Lysates of HEK293T cells were incubated with HDAC1 (**C**), EZH2 (**D**) or SUPT16H (**E**) antibodies. Immunoprecipitated protein samples were analyzed by protein immunoblotting using the indicated antibodies. (F–H) HEK293T cells treated with JQ1 (**F**), UMB-136 (**G**) or CBL0137 (500 nM) (**H**) were subjected to protein immunoblotting analysis of SUPT16H, HDAC1 and phospho-HDAC1 (ser421/423). (I–L) HEK293T cells stably expressing BRD4 or NT shRNA (**I**) were subjected to protein immunoblotting analysis of SUPT16H, HDAC1 and phospho-HDAC1 (ser421/423). The similar analysis as in (**I**) was performed for HEK293T cells transfected with BRD4 (**J**) or SUPT16H (**L**) siRNAs. Knockdown of SUPT16H by its siRNAs was confirmed by RT-qPCR to measure its mRNA level (K). (**M**) HEK293T cells treated with CBL0137 at the increasing doses (100, 200, 500 nM) were subjected to protein immunoblotting analysis using histone H3ac or total H3 antibodies. (**N, O**) Lysates of HEK293T cells transfected with SUPT16H or BRD4 siRNAs were crosslinked and incubated with HDAC1, phospho-HDAC1 (ser421/423), EZH2 antibodies, or control IgG. Immunoprecipitated DNA samples were analyzed by qPCR analysis using primers targeting the promoter region of IFI44L (N) or MX2 (O). Results were calculated from three independent experiments (**** $P < 0.0001$, one-way ANOVA for **K,** two-way ANOVA for N, O).

both HEK293T (Figure 5H, Supplementary Figure S5E) and NK-92 cells (Figure 5I, Supplementary Figure S5F). This is consistent with the other findings that treatment of CBL0137 induces the expression of IFNs and ISGs in NK-92 cells (Supplementary Figure S7). However, it was reported that expression of HERVs or non-coding repetitive elements may trigger IFN response via formation of dsRNA (54,55). Results showed that CBL0137 has a weak effect on inducing dsRNA in contrast with ZIKA infection as a positive control (Supplementary Figure S6G). Upon activation due to dsRNA sensing, RIG-I-like receptors (RLRs) and Toll-like receptor 3 (TLR3) are known to trigger the common downstream factors, TBK1 and IRF3, leading to induction of IFN signaling (56). We further tested the effect of two TBK1 specific inhibitors, amlexanox (57) and GSK8612 (58), on CBL0137-induced expression of IFNs/ISGs (Supplementary Figure S6H). Results showed that both two inhibitors have no obvious effect on abolishing such an effect of CBL0137 in NK-92 cells (Supplementary Figure S6I), supporting that FACT-mediated, direct epigenetic control may play a more significant role in silencing IFNs/ISGs. In conclusion, we provided evidence that FACT subunit SUPT16H suppresses IFN signaling and CBL0137 blocks such effect.

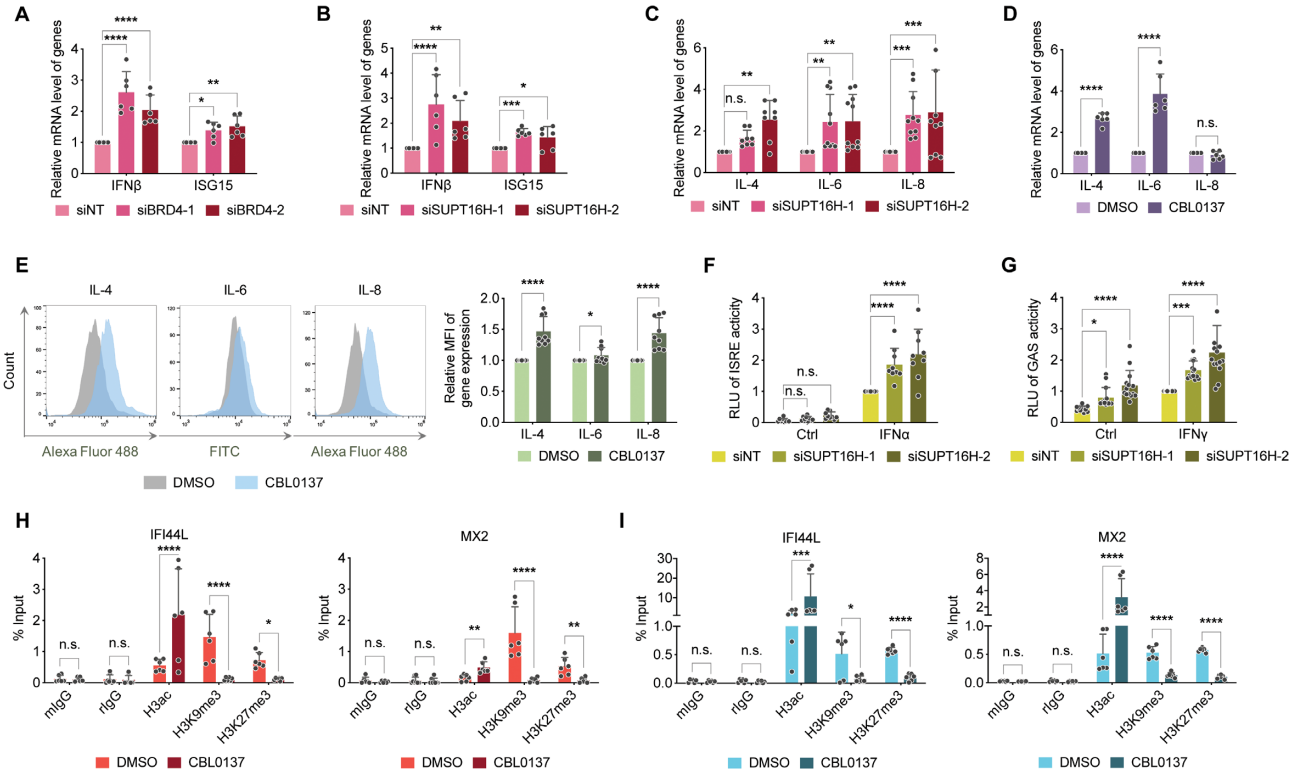

Figure 5. SUPT16H-BRD4 suppresses gene expression of IFN signaling. (A, B) HEK293T cells transfected with BRD4 (**A**) or SUPT16H (**B**) siRNAs were subjected to mRNA RT-qPCR analysis of IFNβ and ISG15 expression. (**C**) HEK293T cells transfected with SUPT16H or NT siRNAs were subjected to mRNA RT-qPCR analysis of IL-4/6/8 expression. (D, E) NK-92 cells treated with CBL0137 (500 nM) were subjected to mRNA RT-qPCR (**D**) or protein immunofluorescence (**E**) analysis of IL-4/6/8 expression. (F, G) HEK293T cells transfected with SUPT16H or NT siRNAs were further transfected with an ISRE-driven (**F**) or GAS-driven (**G**) firefly luciferase reporter plus TK-driven *Renilla* luciferase control vectors, which were stimulated by Type I (IFNα) or II (IFNγ) IFNs, respectively. Relative luciferase unit, RLU (firefly/*Renilla* luciferase activity) from above cells was calculated and normalized to that of siNT-transfected, IFN-treated cells. (H, I) Lysates of HEK293T (**H**) or NK-92 (**I**) cells treated with CBL0137 (500 nM) were crosslinked and incubated with H3ac, H3K9me3, H3K27me3 antibodies or normal IgGs. Immunoprecipitated DNA samples were analyzed by qPCR analysis using primers targeting the promoter region of ISGs (IFI44L, MX2). Results were calculated from three independent experiments (* $P < 0.05$, ** $P < 0.01$, *** $P < 0.001$, **** $P < 0.0001$, two-way ANOVA).

CBL0137 induces IFN signaling and restricts viral infection

IFN signaling plays a central role in host defense against viral infection. Since the SUPT16H inhibitor CBL0137 has the potency to induce IFN signaling, we expected that it can be used as a novel antiviral agent. We first confirmed that knockdown of SUPT16H by its siRNAs (Figure 6A and B) or its inhibition by CBL0137 (Figure 6C) upregulates the expression of IFN genes in HeLa cells. Particularly, IFNγ, the first characterized and broad-spectrum antiviral cytokine, was significantly induced in CBL0137-treated HeLa cells measured by immunofluorescence and flow cytometry (Figure 6D). Induction of selected ISGs (IFI16, MX1, ISG15) in CBL0137-treated HeLa cells was alternatively verified by protein immunoblotting (Figure 6E). We next determined the antiviral effect of SUPT16H depletion or inhibition on various viruses. Interestingly, knockdown of SUPT16H with its siRNAs (Figure 6F) or treatment with CBL0137 (Figure 6G) efficiently blocked the infection of ZIKV. Similarly, knockdown of SSRP1 inhibited ZIKV infection (Supplementary Figure S2E, F), also likely due to its impact on SUPT16H (Supplementary Figure S2B). CBL0137 also exerted the inhibitory effect on infection of influenza A in both HeLa (Figure 6H) and A549 cells (Supplementary Figure S8A). Since SARS-CoV-2 is a newly emerging coronavirus that causes a global threat, we further tested the antiviral effect of CBL0137 on this virus by using the highly reproducible plaque reduction microneutralization (PRMNT) assay (Figure 6I). Indeed, treatment of CBL0137 led to the strong inhibition of SARS-CoV-2 infection in Vero E6 cells, comparable to remdesivir (Figure 6J). Additionally, JQ1 also exhibited the moderate anti-SARS-CoV-2 effect (Supplementary Figure S8B). On the contrary, infection of a DNA virus, Kaposi's sarcoma-associated herpesvirus (KSHV), was not affected by CBL0137 (Supplementary Figure S8C), indicating the different sensitivity of DNA versus RNA viruses to antiviral innate immunity. Therefore, our results demonstrated that CBL0137, a promising anticancer drug currently in clinical trials, also potently induces IFN signaling and inhibits infections of diverse viruses, including SARS-CoV-2, in epithelial cells.

CBL0137 induces NK-mediated killing of virus-infected cells

We demonstrated that SUPT16H acetylation occurs in NK-92 cells (Figure 1A). We also observed that treatment of CBL0137 affects gene expression of selected ISGs in

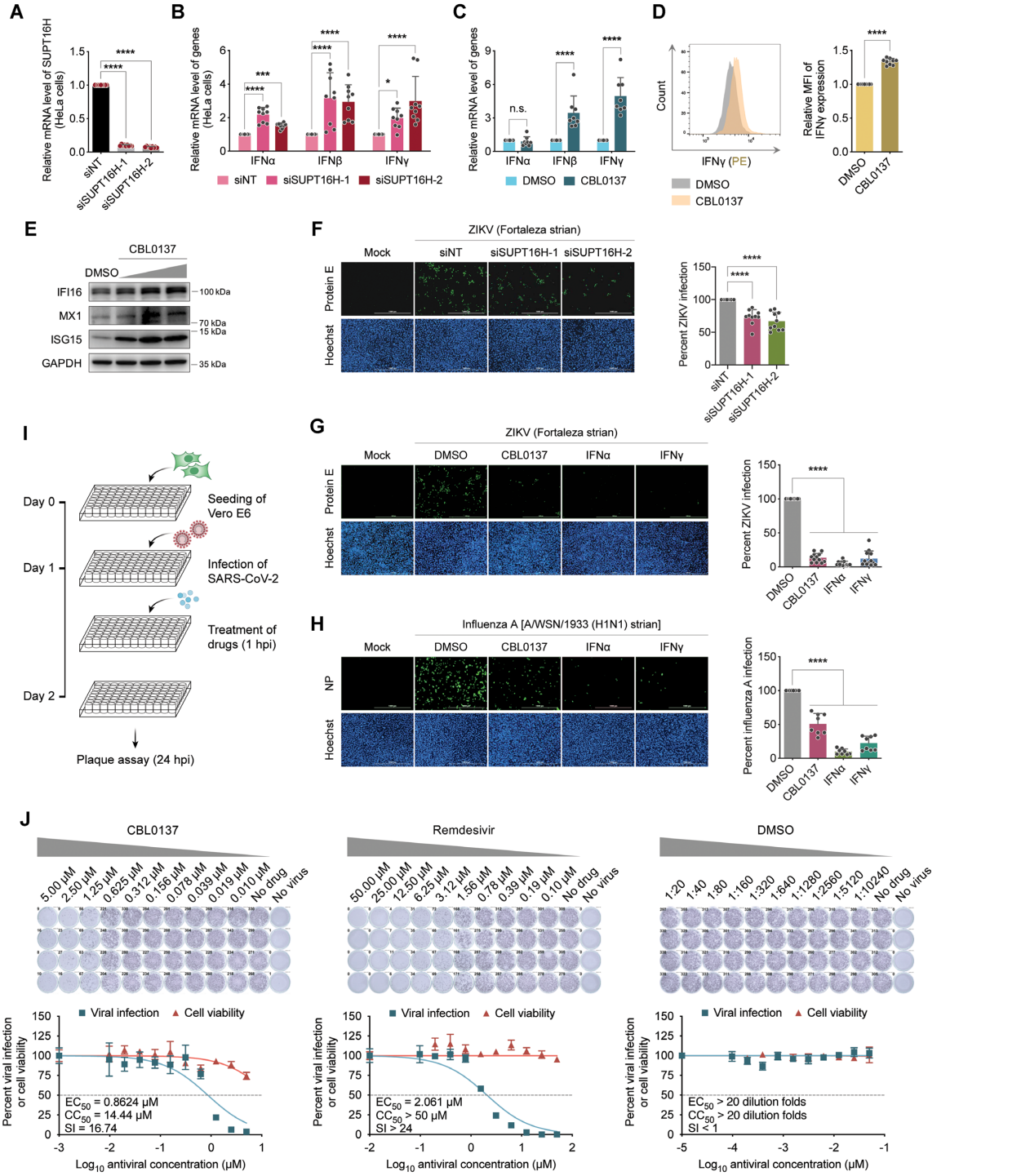

Figure 6. CBL0137 induces IFN signaling and restricts viral infection. (A, B) HeLa cells transfected with SUPT16H or NT siRNAs were subjected to mRNA RT-qPCR analysis of SUPT16H (**A**) or IFNs (**B**) expression. (**C**) HeLa cells treated with CBL0137 (500 nM) were subjected to mRNA RT-qPCR analysis of IFNs expression. (**D**) HeLa cells treated with CBL0137 (500 nM) were subjected to protein immunofluorescence analysis of IFNγ by flow cytometry, and results were normalized to DMSO. (**E**) HeLa cells treated with CBL0137 at the increasing doses (100, 200, 500 nM) were subjected to protein immunoblotting analysis of ISGs using the indicated antibodies. (**F**) HeLa cells were transfected with SUPT16H or NT siRNAs, followed by mock infection (no viruses) or viral infection of ZIKV (MOI = 0.5). At 48 hpi, cells were subjected to protein immunofluorescence analysis of ZIKV protein E. Viral infection rate was calculated and normalized to that of siNT-transfected cells. (G, H) HeLa cells were treated with CBL0137 or IFNs (IFNα or IFNγ), followed by mock infection or viral infection of ZIKV (**G**) or influenza A (**H**) virus (MOI = 0.5). At 48 hpi (ZIKV) or 24 hpi (influenza A), the above cells were subjected to protein immunofluorescence analysis of viral protein (ZIKV: protein E; influenza A: NP). (**I**) Schematic illustration of PRMNT assay for SARS-CoV-2 infection. (**J**) Vero E6 cells were infected with SARS-CoV-2 (100–200 PFU/well), followed by treatment of 2-fold serial dilutions of the indicated compounds (CBL0137, remdesivir, or DMSO). At 24 hpi, the above cells were subjected to PRMNT assay at four biological replicates. Results were calculated from three independent experiments (*** $P < 0.001$, **** $P < 0.0001$, Student's *t*-test for D, one-way ANOVA for A, F, G, H, two-way ANOVA for B, C).

NK-92 cells (Supplementary Figure S7). Thus, we further investigated the impact of the SUPT16H inhibitor CBL0137 on induction of IFN signaling in NK cells. We first performed RNA-seq assays for CBL0137-treated NK-92 cells, which revealed that CBL0137 causes the systemic upregulation of IFNs and ISGs with statistical significance (Figure 7A). For selected ISGs upregulated by CBL0137, there was a strong correlation of RNA-seq and RT-qPCR results (Figure 7B and C, Supplementary Figure S7). Pathway analysis confirmed that certain gene sets are enriched from RNA-seq assays of CBL0137-treated NK-92 cells, including responses to virus, IFNγ and type I IFNs (Figure 7D). We also performed the similar analysis for previously published RNA-seq datasets of CBL0137-treated MV4-11 acute myeloid leukemia (AML) cells (24), which resulted in the similar finding that CBL0137 significantly induces the expression of cellular genes enriched in IFN signaling (Supplementary Figure S9). This is important, since it indicated that CBL0137 effect on IFN signaling is a universal event independent of cell types. Since IFNs production, especially IFNγ, is a hallmark of NK cell activation, we next determined the impact of CBL0137 on cell killing functions of NK cells. In the well-established NK-92 and K562 co-culture assays (Supplementary Figure S10), treatment of NK-92 cells with CBL0137 caused the drastic increase of CD107a and IFNγ expression with the stimulation of K562 cells (Figure 7E). Finally, we evaluated the effect of SUPT16H depletion or inhibition on boosting NK cell-mediated killing of virus-infected cells using ZIKV as an example (Figure 7F). Knockdown of SUPT16H by its siRNAs (Figure 7G and H) or treatment of CBL0137 (Figure 7I) in NK-92 cells indeed enhanced NK cell-mediated killing of ZIKV-infected HeLa cells. More importantly, we observed the similar effect of CBL0137 by using primary NK cells isolated from peripheral blood mononuclear cells (PBMCs) of healthy donors (Figure 7J). Knockdown of SSRP1 by its siRNAs also increased NK cell-mediated killing of ZIKV-infected HeLa cells (Supplementary Figure S2G–J), likely due to its impact on SUPT16H (Supplementary Figure S2B). To summarize, our results demonstrated that beyond the antiviral effect on epithelial cells directly infected with viruses, depletion or inhibition of SUPT16H is also capable of inducing IFN signaling and thus activating NK cells to execute the killing of virus-infected epithelial cells, adding another layer of therapeutic potential of CBL0137 to treat viral infections.

DISCUSSION

Histone chaperones play the key roles in regulating chromatin dynamics, especially nucleosome turnover and gene expression (1). Different from most histone chaperones, FACT complex targets both H2A–H2B dimer and H3–H4 tetramer to equilibrate the assembly/disassembly of nucleosomes, through extensive interactions with histones and nucleosomal DNAs (59). SUPT16H is a key subunit of FACT complex and a large protein that mediates the majority of above protein interactions (59,60). There is evidence that FACT complex possesses both positive and negative regulations of gene expression, but FACT-mediated gene silencing function has not been well characterized comparing to its transactivation activity. In this study, we reported a novel mechanism granting FACT the gene suppression function (Figure 8). We identified that FACT subunit SUPT16H undergoes acetylation, catalyzed by TIP60, and interacts with the acetylation 'reader' BRD4, which prevents the protein degradation of SUPT16H. SUPT16H-BRD4 further associates with epigenetic silencing enzymes, including the 'eraser' HDAC1 and 'writer' EZH2, and regulates their activation status and/or promoter association, which contributes to functional overlaps of SUPT16H and BRD4 to suppress gene expression. Furthermore, our studies recognized that cellular genes involved in IFN signaling are the new gene targets subjected to modulation of SUPT16H-BRD4. At last, we demonstrated that the SUPT16H inhibitor CBL0137 is potent to induce IFN signaling in both epithelial and NK cells, forming two host defense layers against viral infections.

FACT is a multifunctional protein complex, and previous studies have proposed several distinct mechanisms explaining FACT-mediated suppression of gene expression, such as genes with cryptic promoters. FACT was reported to suppress transcription initiation of cryptic promoters by maintaining normal chromatin structure during transcription elongation (11,61). FACT may also suppress expression from cryptic promoters through a 'side-effect' of chromatin reassembly, since chromatin reassembly due to the role of FACT causes histone deacetylation (5,62). In addition, FACT may repress cryptic promoters through other epigenetic regulators beside its role as a chromatin chaperone (13). Above evidence suggests that FACT likely has both the passive and active roles in silencing gene expression. Furthermore, we provided the evidence that SUPT16H associates with the promoter region of ISGs/IFNs, and influences binding and/or activity of epigenetic regulators (HDAC1/EZH2) at their loci (Figure 5C and D; Figure 4N, O; A–E). Meanwhile, we also showed that knockdown or inhibition of SUPT16H moderately upregulate the expression of HERVs (Supplementary Figure S6A–F). Induction of HERVs or non-coding repetitive elements may trigger IFN response through the formation of dsRNA (54,55). However, we observed that CBL0137 only has a weak effect on inducing dsRNA formation (Supplementary Figure S6G), and that inhibition of TBK1, a downstream kinase required for dsRNA sensing to activate IFN signaling, has no obvious effect on preventing CBL0137-induced expression of ISGs/IFNs (Supplementary Figure S6H, I). Taken together, our overall results support that FACT suppresses expression of immune genes more likely by directly regulating epigenetic control at their loci versus via dsRNA sensing.

A new and significant finding is that we link the SUPT16H–BRD4–HDAC1 interaction with HDAC1 phosphorylation known to be required for its activation. BRD4 was identified as an atypical kinase (63) that may contribute to HDAC1 phosphorylation, but other kinases associating with SUPT16H-BRD4 may also be involved. However, comparing to HDAC1, EZH2 phosphorylation is more complicated, since multiple phosphorylation sites of EZH2 have been reported, which either inhibit or activate its methyl-transferase activity, such as ser21 and thr492 (64,65) or thr350 (66) respectively. Thus, impact

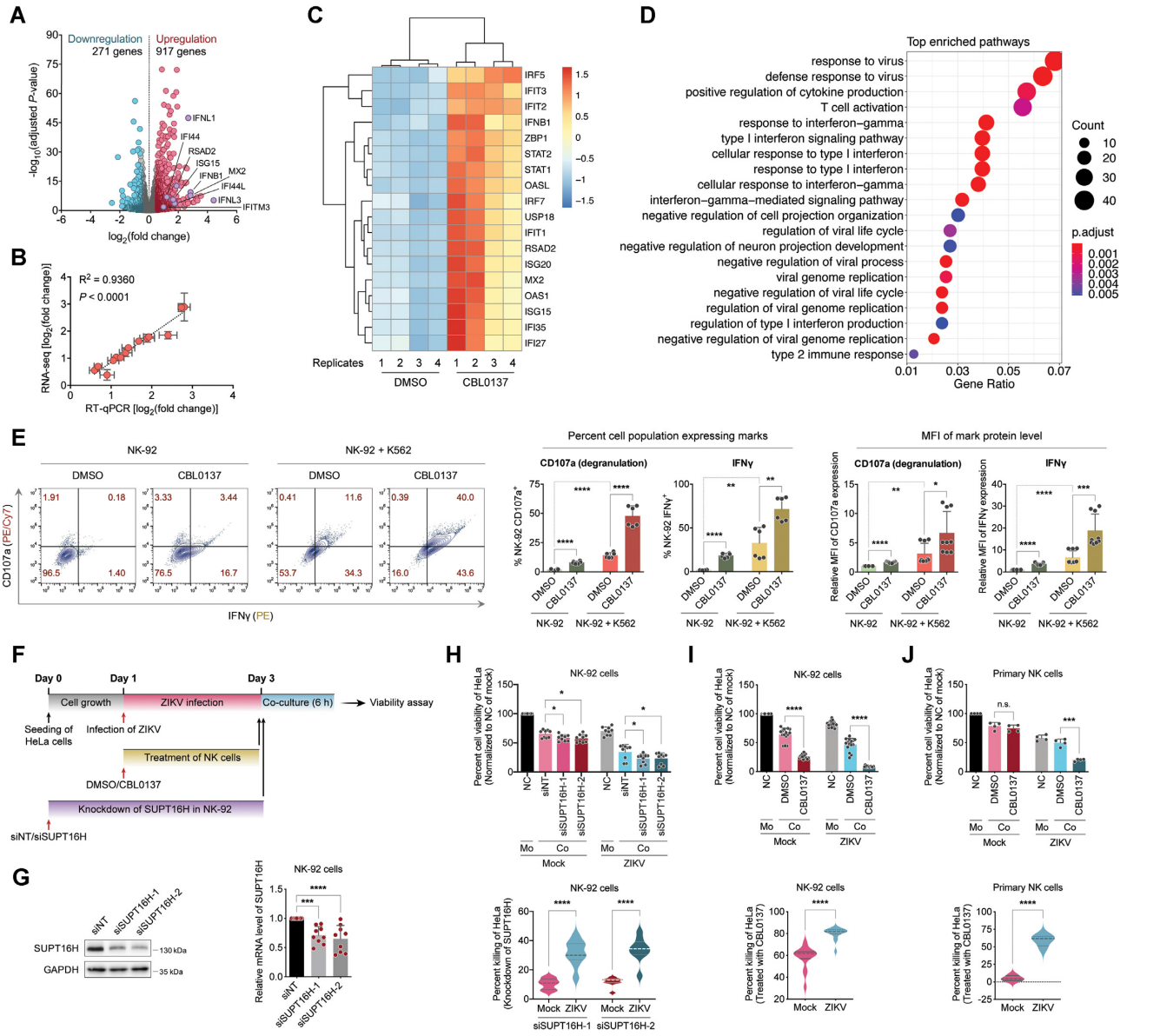

Figure 7. CBL0137 activates NK cell-mediated killing of virus-infected cells. (**A**) Total RNAs were extracted from NK-92 cells treated with CBL0137 (500 nM) or DMSO at four independent replicates, and subjected to RNA-seq analysis. A volcano plot was constructed for RNA-seq results. (**B**) Correlation between RNA-seq and RT-qPCR data for the selected ISGs was determined by Pearson's *r* with statistical significance. (**C**) Upregulation of selected ISGs in RNA-seq data of NK-92 cells treated with CBL0137 was illustrated in a heatmap (R package: pheatmap). (**D**) Pathway analysis was performed for RNA-seq data of NK-92 cells treated with CBL0137 using GO biological process (BP) (R package: clusterProfiler). (**E**) NK-92 cells treated with CBL0137 (500 nM) or DMSO were co-cultured with or without K562 cells, followed by the protein immunofluorescence analysis of CD107a or IFNγ in NK-92 cells by flow cytometry. Percentage of cell population expressing CD107a or IFNγ as well as the mean fluorescence intensity (MFI) of CD107a or IFNγ were calculated and normalized to DMSO without K562 stimulation. (**F**) Schematic illustration of the procedure to measure NK cell-mediated killing of ZIKV-infected cells. (**G**) Knockdown of SUPT16H by its siRNAs in NK-92 cells was confirmed by both protein immunoblotting and RT-qPCR. (H–J) NK-92 cells transfected with SUPT16H or NT siRNAs (**H**), treated with CBL0137 (500 nM) or DMSO (**I**), or primary NK cells treated with CBL0137 (500 nM) or DMSO (**J**), were co-cultured with mock or ZIKV-infected HeLa cells. Viability of HeLa cells was measured by using ATP-based assay (upper panel), and converted to cell killing efficacy (lower panel, lines in plots indicate median and 25%/75% percentile). Viability of HeLa cells without co-culture with NK cells nor ZIKV infection was set as 100% (NC: negative control; Mo: mono-culture of HeLa; Co: co-culture of HeLa with NK). Results were calculated from four biological replicates for **J**, and three independent experiments for all others (* $P < 0.05$, ** $P < 0.01$, *** $P < 0.001$, **** $P < 0.0001$, two-way ANOVA for H–J [upper panel], E, and Student's *t*-test for H–J [lower panel]).

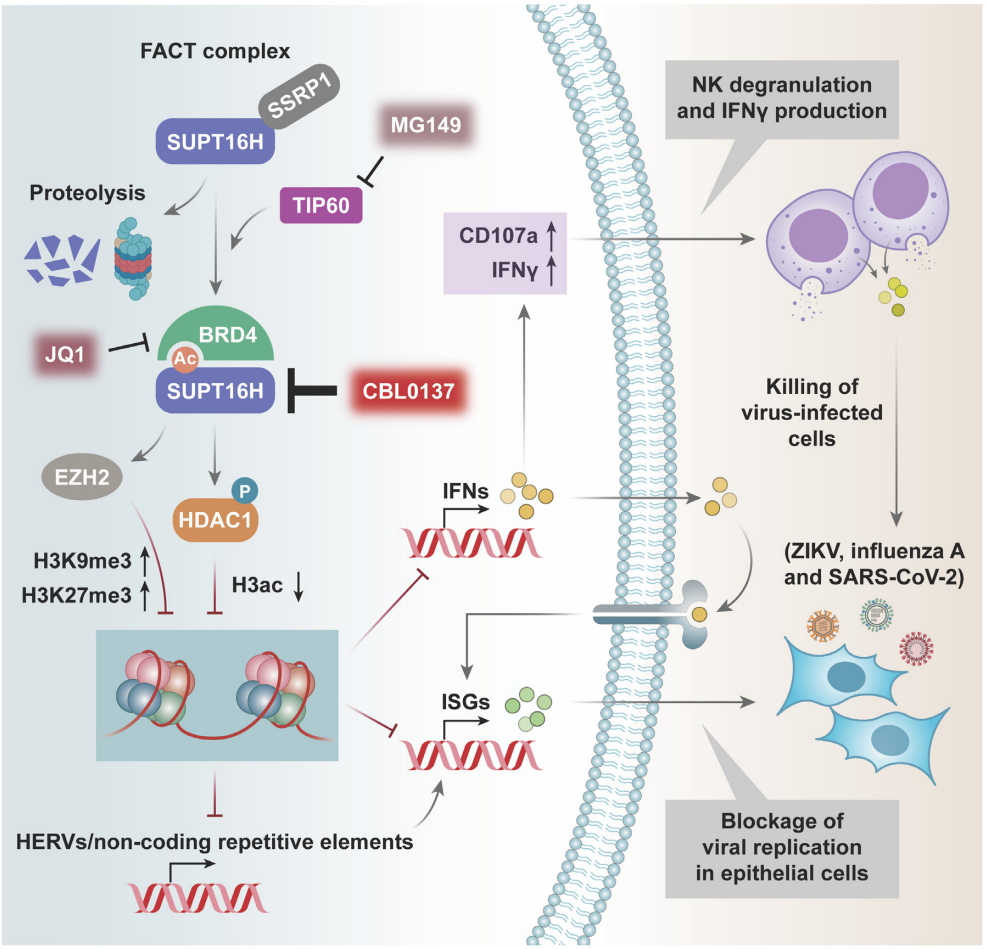

Figure 8. SUPT16H–BRD4 function of gene suppression in antiviral IFN signaling. FACT subunit SUPT16H undergoes protein acetylation at K674 of MD domain, catalyzed by TIP60, which is recognized by BRD4. Such SUPT16H–BRD4 interaction prevents the protein degradation of SUPT16H. SUPT16H–BRD4 physically associates with epigenetic silencing enzymes (HDAC1, EZH2), and further affects their activation status and/or promoter association as well as modulates the histone marks (H3ac, H3K9me3, H3K27me3), which overall results in the functional overlaps of SUPT16H and BRD4 to suppress gene expression, including HERVs, non-coding repetitive elements, IFNs, and ISGs, in multiple types of cells, such as epithelial and NK cells. Furthermore, the SUPT16H inhibitor CBL0137 is potent to induce IFN signaling in both epithelial and NK cells, forming two host defense layers against viral infections.

of SUPT16H–BRD4 on EZH2 phosphorylation could be profound. But we did notice that the promoter association of total EZH2 is indeed dependent on SUPT16H-BRD4, which would impact the level of histone methylation marks (H3K27/K9me3).

Although our own data as well as some earlier studies showed that BRD4 is similar as SUPT16H to suppress gene expression in IFN signaling and that treatment of JQ1 induces expression of IFN and ISGs (50,51), there are also other studies reporting that BRD4 plays an opposite role. For example, BRD4 has been reported to coordinate with NF-κB/RelA that leads to the activation of IFN signaling and inflammatory responses (67,68). BRD4 may also participate in the positive regulation of gene expression through the recruitment of P-TEFb (69). A plausible explanation of such paradox is that BRD4 likely recognizes other acetylated protein targets, so that its depletion or inhibition may create a more profound impact. BRD4 interaction with acetylated protein targets, including SUPT16H, would rather be dynamic and highly dependent on cellular environment and activation status, which would overall influence BRD4's function in gene regulation. Thus, BRD4 may disconnect from SUPT16H in terms of their gene suppression function although they interact with each other. Such discrepancy could occur across different cell types and conditions. However, we observed that treatment of CBL0137 causes the fairly consistent impact on inducing IFN signaling in different cell types, indicating that SUPT16H may play a more robust role in silencing IFN and ISGs than BRD4.

Beyond IFN signaling, earlier studies reported that BRD4 also regulates viral infection through other IFN-independent mechanisms. BRD4 affects infection of human papillomaviruses (HPVs) both positively and negatively (70,71). Likewise, BRD4 also profoundly impacts HIV-1 transcription and latency. BRD4 was initially identified to promote HIV-1 transcription (72), but was subsequently confirmed as a HIV-1 latency-promoting gene (73). Inhibition of BRD4 was reported to either activate (42,74) or inhibit (75) HIV-1 latent reactivation. Both BRD4L

and BRD4S have been reported to silence HIV-1 proviral expression through different mechanisms. Our earlier results showed that BRD4L competes with HIV-1 Tat protein for P-TEFb binding and thus suppresses Tat-mediated transcriptional elongation (42). However, BRD4S was also reported to suppresses replication of HPVs and HIV-1 (76,77), likely through hijacking SWI/SNF chromatin-remodeling complex (76). Our results showed that only BRD4L binds to SUPT16H (Figure 1F, and G; Supplementary Figure S3A), indicating that SUPT16H regulates gene silencing mainly through BRD4L. Interestingly, BRD4S has the similar structure as BRD2 with both lacking C-terminal extension, which may explain our finding that BRD2 has no protein interaction with SUPT16H nor affect its protein level (Figure 1G, Supplementary Figure S4C). It is still under debate whether BRD4L and BRD4S truly behave distinctly or function with certain overlaps. Several publications reported the distinct roles of these BRD4 isoforms, such as in cancer development (38), DNA damage (78), and viral life cycle (76). However, there are also other publications showing that BRD4L acts as either an activator or a repressor of gene expression (72,79). These results suggested that the functions of BRD4 isoforms are not absolutely identical in different scenarios, and might include different mechanisms. Our studies identified the interaction of SUPT16H-BRD4 with epigenetic factors (HDAC1, EZH2), which may present a new mechanism for BRD4L to regulate gene expression. Our work can clearly conclude that SUPT16H interacts with BRD4L, but it is still uncertain whether BRD4S is involved as well, which needs future, more detailed investigation.

In addition, our results further showed that the acetylated MD domain of SUPT16H preferentially binds to BD1 versus BD2 (Supplementary Figure S3D), indicating the different binding capacity of BRD4's two bromodomains. These data support the earlier finding that the BRD4–BD1 and BD2 possess distinct binding specificities with the same acetylated protein (35). It is likely that such discrepancy in binding efficiency is due to the substantial sequence diversity existing among bromodomains (80), which also explains that the BET family proteins (BRD2, BRD3, BRD4 and BRDT) possess the different patterns of bromodomain-dependent interactions with the acetylated proteins.

Prior to our studies, there were some reports indicating the potential role of other histone chaperones, but not FACT complex, in regulating IFN signaling (81,82). Our results provided new evidence to link FACT complex with silencing of IFN signaling, which extends our knowledge regarding its profound modulatory activities. Our results also bear translational significance by illustrating the new effect of CBL0137 on IFNs induction. Numerous studies have demonstrated the anticancer potential of CBL0137 through regulation of NF-κB pathway (83–85). Identification of CBL0137's effect on IFNs activation would further guide its application for treating cancers via immunomodulation. On the contrary, CBL0137's antiviral potential has never been explored. Our results showed that CBL0137 exerts the antiviral activities in both non-immune (epithelial) and immune (NK) cells, which is worthy of further *in vivo* evaluation, since CBL0137 has already been investigated in animal models of certain cancers (83,85,86) and advanced to clinical trials. Particularly, CBL0137 can be considered as a new broad antiviral drug candidate against SARS-CoV-2, since there are so far still few effective antiviral therapies for treating this devastating virus that causes the global COVID-19 pandemic.

DATA AVAILABILITY

RNA-seq data are deposited in Gene Expression Omnibus (GEO) with the accession number GSE184784. Flow cytometry data are deposited in FLOWRepository with the repository IDs FR-FCM-Z4K4, FR-FCM-Z4K6 and FR-FCM-Z4K7. The datasets of ChIP-seq analyzed in this study are from GEO with the accession numbers GSE117333 (SUPT16H) and GSE151015 (BRD4). The custom codes for ChIP-seq data analysis are deposited at GitHub with the following link: https://github.com/ZhenyuWu-OSU/SPT16_BRD4-CHIP-seq.

All data are present in the main paper or as the supplementary materials. All other related data, information and materials can be acquired through the specific request.

SUPPLEMENTARY DATA

Supplementary Data are available at NAR Online.

ACKNOWLEDGEMENTS

We thank Wei Zhang (University of Massachusetts at Boston) for providing UMB-136, a BETi derived from 3,5-dimethylisoxazole BETi UMB-32 (87).

Author contributions: J.Z. and D.Z. conceived and designed this study; D.Z. performed most of the experiments; Z.W. performed the pathway analysis and heatmap construction for RNA-seq and ChIP-seq analysis. J.G.P. performed the PRMNT assay and its data processing; D.Z., N.G.S. and J.Z. analyzed the results; Z.W., J.G.P., G.N.F., T.L., Q.M., H.H., A.B. and L.M.S. contributed materials and/or provided advice for this study; D.Z., Z.W. and J.Z. wrote the manuscript; J.Z. supervised the entire study.

FUNDING

NIH [R01AI150448, R01DE025447, R56AI157872 to J.Z., R01CA260690, R03DE029716 to N.G.S.]. Funding for open access charge: NIH and/or OSU funding.

Conflict of interest statement. None declared.

REFERENCES

1. Hammond,C.M., Stromme,C.B., Huang,H., Patel,D.J. and Groth,A. (2017) Histone chaperone networks shaping chromatin function. *Nat. Rev. Mol. Cell Biol.*, **18**, 141–158.
2. Orphanides,G., LeRoy,G., Chang,C.H., Luse,D.S. and Reinberg,D. (1998) FACT, a factor that facilitates transcript elongation through nucleosomes. *Cell*, **92**, 105–116.
3. Belotserkovskaya,R., Oh,S., Bondarenko,V.A., Orphanides,G., Studitsky,V.M. and Reinberg,D. (2003) FACT facilitates transcription-dependent nucleosome alteration. *Science*, **301**, 1090–1093.
4. Stuwe,T., Hothorn,M., Lejeune,E., Rybin,V., Bortfeld,M., Scheffzek,K. and Ladurner,A.G. (2008) The FACT spt16 "peptidase" domain is a histone H3-H4 binding module. *Proc. Natl. Acad. Sci. U.S.A.*, **105**, 8884–8889.

5. Formosa,T. and Winston,F. (2020) The role of FACT in managing chromatin: disruption, assembly, or repair?*Nucleic Acids Res.*, **48**, 11929–11941.
6. Murawska,M. and Ladurner,A.G. (2016) CENPs and sweet nucleosomes face the FACT. *Trends Biochem. Sci.*, **41**, 736–738.
7. Wienholz,F., Zhou,D., Turkyilmaz,Y., Schwertman,P., Tresini,M., Pines,A., van Toorn,M., Bezstarosti,K., Demmers,J.A.A. and Marteijn,J.A. (2019) FACT subunit spt16 controls UVSSA recruitment to lesion-stalled RNA pol II and stimulates TC-NER. *Nucleic Acids Res.*, **47**, 4011–4025.
8. Ding,Q., He,K., Luo,T., Deng,Y., Wang,H., Liu,H., Zhang,J., Chen,K., Xiao,J., Duan,X. *et al.* (2016) SSRP1 contributes to the malignancy of hepatocellular carcinoma and is negatively regulated by miR-497. *Mol. Ther.*, **24**, 903–914.
9. Huang,H., Santoso,N., Power,D., Simpson,S., Dieringer,M., Miao,H., Gurova,K., Giam,C.Z., Elledge,S.J. and Zhu,J. (2015) FACT proteins, SUPT16H and SSRP1, are transcriptional suppressors of HIV-1 and HTLV-1 that facilitate viral latency. *J. Biol. Chem.*, **290**, 27297–27310.
10. Guo,R., Jiang,C., Zhang,Y., Govande,A., Trudeau,S.J., Chen,F., Fry,C.J., Puri,R., Wolinsky,E., Schineller,M. *et al.* (2020) MYC controls the Epstein-Barr virus lytic switch. *Mol. Cell*, **78**, 653–669.
11. Kaplan,C.D., Laprade,L. and Winston,F. (2003) Transcription elongation factors repress transcription initiation from cryptic sites. *Science*, **301**, 1096–1099.
12. Murawska,M., Schauer,T., Matsuda,A., Wilson,M.D., Pysik,T., Wojcik,F., Muir,T.W., Hiraoka,Y., Straub,T. and Ladurner,A.G. (2020) The chaperone FACT and histone H2B ubiquitination maintain s. pombe genome architecture through genic and subtelomeric functions. *Mol. Cell*, **77**, 501–513.
13. Chen,F., Zhang,W., Xie,D., Gao,T., Dong,Z. and Lu,X. (2020) Histone chaperone FACT represses retrotransposon MERVL and MERVL-derived cryptic promoters. *Nucleic Acids Res.*, **48**, 10211–10225.
14. Han,J., Li,Q., McCullough,L., Kettelkamp,C., Formosa,T. and Zhang,Z. (2010) Ubiquitylation of FACT by the cullin-E3 ligase rtt101 connects FACT to DNA replication. *Genes Dev.*, **24**, 1485–1490.
15. Choudhary,C., Kumar,C., Gnad,F., Nielsen,M.L., Rehman,M., Walther,T.C., Olsen,J.V. and Mann,M. (2009) Lysine acetylation targets protein complexes and co-regulates major cellular functions. *Science*, **325**, 834–840.
16. Beli,P., Lukashchuk,N., Wagner,S.A., Weinert,B.T., Olsen,J.V., Baskcomb,L., Mann,M., Jackson,S.P. and Choudhary,C. (2012) Proteomic investigations reveal a role for RNA processing factor THRAP3 in the DNA damage response. *Mol. Cell*, **46**, 212–225.
17. Mertins,P., Qiao,J.W., Patel,J., Udeshi,N.D., Clauser,K.R., Mani,D.R., Burgess,M.W., Gillette,M.A., Jaffe,J.D. and Carr,S.A. (2013) Integrated proteomic analysis of post-translational modifications by serial enrichment. *Nat. Methods*, **10**, 634–637.
18. Weinert,B.T., Scholz,C., Wagner,S.A., Iesmantavicius,V., Su,D., Daniel,J.A. and Choudhary,C. (2013) Lysine succinylation is a frequently occurring modification in prokaryotes and eukaryotes and extensively overlaps with acetylation. *Cell Rep.*, **4**, 842–851.
19. Huang,H., Kong,W., Jean,M., Fiches,G., Zhou,D., Hayashi,T., Que,J., Santoso,N. and Zhu,J. (2019) A CRISPR/Cas9 screen identifies the histone demethylase MINA53 as a novel HIV-1 latency-promoting gene (LPG). *Nucleic Acids Res.*, **47**, 7333–7347.
20. Zhou,D., Hayashi,T., Jean,M., Kong,W., Fiches,G., Biswas,A., Liu,S., Yosief,H.O., Zhang,X., Bradner,J. *et al.* (2020) Inhibition of Polo-like kinase 1 (PLK1) facilitates the elimination of HIV-1 viral reservoirs in CD4(+) t cells ex vivo. *Sci. Adv.*, **6**, eaba1941.
21. Biswas,A., Zhou,D., Fiches,G.N., Wu,Z., Liu,X., Ma,Q., Zhao,W., Zhu,J. and Santoso,N.G. (2021) Inhibition of polo-like kinase 1 (PLK1) facilitates reactivation of gamma-herpesviruses and their elimination. *PLoS Pathog.*, **17**, e1009764.
22. Fiches,G.N., Wu,Z., Zhou,D., Biswas,A., Li,T.W., Kong,W., Jean,M., Santoso,N.G. and Zhu,J. (2022) Polyamine biosynthesis and eIF5A hypusination are modulated by the DNA tumor virus KSHV and promote KSHV viral infection. *PLoS Pathog.*, **18**, e1010503.
23. Love,M.I., Huber,W. and Anders,S. (2014) Moderated estimation of fold change and dispersion for RNA-seq data with DESeq2. *Genome Biol.*, **15**, 550.
24. Somers,K., Kosciolek,A., Bongers,A., El-Ayoubi,A., Karsa,M., Mayoh,C., Wadham,C., Middlemiss,S., Neznanov,N., Kees,U.R. *et al.* (2020) Potent antileukemic activity of curaxin CBL0137 against MLL-rearranged leukemia. *Int. J. Cancer*, **146**, 1902–1916.
25. Qin,Q., Mei,S., Wu,Q., Sun,H., Li,L., Taing,L., Chen,S., Li,F., Liu,T., Zang,C. *et al.* (2016) ChiLin: a comprehensive chip-seq and DNase-seq quality control and analysis pipeline. *BMC Bioinformatics*, **17**, 404.
26. Karczewski,K.J., Tatonetti,N.P., Landt,S.G., Yang,X., Slifer,T., Altman,R.B. and Snyder,M. (2011) Cooperative transcription factor associations discovered using regulatory variation. *Proc. Natl. Acad. Sci. U.S.A.*, **108**, 13353–13358.
27. Matsuda,K., Mikami,T., Oki,S., Iida,H., Andrabi,M., Boss,J.M., Yamaguchi,K., Shigenobu,S. and Kondoh,H. (2017) ChIP-seq analysis of genomic binding regions of five major transcription factors highlights a central role for ZIC2 in the mouse epiblast stem cell gene regulatory network. *Development*, **144**, 1948–1958.
28. Pugacheva,E.M., Kubo,N., Loukinov,D., Tajmul,M., Kang,S., Kovalchuk,A.L., Strunnikov,A.V., Zentner,G.E., Ren,B. and Lobanenkov,V.V. (2020) CTCF mediates chromatin looping via N-terminal domain-dependent cohesin retention. *Proc. Natl. Acad. Sci. U.S.A.*, **117**, 2020–2031.
29. Garrido,C., Abad-Fernandez,M., Tuyishime,M., Pollara,J.J., Ferrari,G., Soriano-Sarabia,N. and Margolis,D.M. (2018) Interleukin-15-stimulated natural killer cells clear HIV-1-Infected cells following latency reversal ex vivo. *J. Virol.*, **92**, e00235–18.
30. Park,J.G., Oladunni,F.S., Chiem,K., Ye,C., Pipenbrink,M., Moran,T., Walter,M.R., Kobie,J. and Martinez-Sobrido,L. (2021) Rapid in vitro assays for screening neutralizing antibodies and antivirals against SARS-CoV-2. *J. Virol. Methods*, **287**, 113995.
31. John,S., Howe,L., Tafrov,S.T., Grant,P.A., Sternglanz,R. and Workman,J.L. (2000) The something about silencing protein, sas3, is the catalytic subunit of nua3, a yTAF(II)30-containing HAT complex that interacts with the spt16 subunit of the yeast CP (Cdc68/Pob3)-FACT complex. *Genes Dev.*, **14**, 1196–1208.
32. Rajagopalan,D., Tirado-Magallanes,R., Bhatia,S.S., Teo,W.S., Sian,S., Hora,S., Lee,K.K., Zhang,Y., Jadhav,S.P., Wu,Y. *et al.* (2018) TIP60 represses activation of endogenous retroviral elements. *Nucleic Acids Res.*, **46**, 9456–9470.
33. Gong,F., Chiu,L.Y. and Miller,K.M. (2016) Acetylation reader proteins: linking acetylation signaling to genome maintenance and cancer. *PLoS Genet.*, **12**, e1006272.
34. Prinjha,R.K., Witherington,J. and Lee,K. (2012) Place your BETs: the therapeutic potential of bromodomains. *Trends Pharmacol. Sci.*, **33**, 146–153.
35. Shi,J., Wang,Y., Zeng,L., Wu,Y., Deng,J., Zhang,Q., Lin,Y., Li,J., Kang,T., Tao,M. *et al.* (2014) Disrupting the interaction of BRD4 with diacetylated twist suppresses tumorigenesis in basal-like breast cancer. *Cancer Cell*, **25**, 210–225.
36. Cheung,K.L., Zhang,F., Jaganathan,A., Sharma,R., Zhang,Q., Konuma,T., Shen,T., Lee,J.Y., Ren,C., Chen,C.H. *et al.* (2017) Distinct roles of brd2 and brd4 in potentiating the transcriptional program for Th17 cell differentiation. *Mol. Cell*, **65**, 1068–1080.
37. Dey,A., Chitsaz,F., Abbasi,A., Misteli,T. and Ozato,K. (2003) The double bromodomain protein brd4 binds to acetylated chromatin during interphase and mitosis. *Proc. Natl. Acad. Sci. U.S.A.*, **100**, 8758–8763.
38. Wu,S.Y., Lee,C.F., Lai,H.T., Yu,C.T., Lee,J.E., Zuo,H., Tsai,S.Y., Tsai,M.J., Ge,K., Wan,Y. *et al.* (2020) Opposing functions of BRD4 isoforms in breast cancer. *Mol Cell*, **78**, 1114–1132.
39. Huang,H., Liu,S., Jean,M., Simpson,S., Huang,H., Merkley,M., Hayashi,T., Kong,W., Rodriguez-Sanchez,I., Zhang,X. *et al.* (2017) A novel bromodomain inhibitor reverses HIV-1 latency through specific binding with BRD4 to promote tat and P-TEFb association. *Front. Microbiol.*, **8**, 1035.
40. Kaja,A., Adhikari,A., Karmakar,S., Zhang,W., Rothschild,G., Basu,U., Batra,S.K., Davie,J.K. and Bhaumik,S.R. (2021) Proteasomal regulation of mammalian SPT16 in controlling transcription. *Mol. Cell Biol.*, **41**, e00452–20.
41. Shen,J., Chen,M., Lee,D., Law,C.T., Wei,L., Tsang,F.H., Chin,D.W., Cheng,C.L., Lee,J.M., Ng,I.O. *et al.* (2020) Histone chaperone FACT complex mediates oxidative stress response to promote liver cancer progression. *Gut*, **69**, 329–342.

42. Zhu,J., Gaiha,G.D., John,S.P., Pertel,T., Chin,C.R., Gao,G., Qu,H., Walker,B.D., Elledge,S.J. and Brass,A.L. (2012) Reactivation of latent HIV-1 by inhibition of BRD4. *Cell Rep*, **2**, 807–816.
43. Gautier,V.W., Gu,L., O'Donoghue,N., Pennington,S., Sheehy,N. and Hall,W.W. (2009) In vitro nuclear interactome of the HIV-1 tat protein. *Retrovirology*, **6**, 47.
44. Prendergast,L., Muller,S., Liu,Y., Huang,H., Dingli,F., Loew,D., Vassias,I., Patel,D.J., Sullivan,K.F. and Almouzni,G. (2016) The CENP-T/-W complex is a binding partner of the histone chaperone FACT. *Genes Dev*, **30**, 1313–1326.
45. Xu,J., Shao,Z., Li,D., Xie,H., Kim,W., Huang,J., Taylor,J.E., Pinello,L., Glass,K., Jaffe,J.D. *et al.* (2015) Developmental control of polycomb subunit composition by GATA factors mediates a switch to non-canonical functions. *Mol. Cell*, **57**, 304–316.
46. Pflum,M.K., Tong,J.K., Lane,W.S. and Schreiber,S.L. (2001) Histone deacetylase 1 phosphorylation promotes enzymatic activity and complex formation. *J. Biol. Chem.*, **276**, 47733–47741.
47. Margueron,R. and Reinberg,D. (2011) The polycomb complex PRC2 and its mark in life. *Nature*, **469**, 343–349.
48. Xu,C., Bian,C., Yang,W., Galka,M., Ouyang,H., Chen,C., Qiu,W., Liu,H., Jones,A.E., MacKenzie,F. *et al.* (2010) Binding of different histone marks differentially regulates the activity and specificity of polycomb repressive complex 2 (PRC2). *Proc. Natl. Acad. Sci. U.S.A.*, **107**, 19266–19271.
49. Mozzetta,C., Pontis,J., Fritsch,L., Robin,P., Portoso,M., Proux,C., Margueron,R. and Ait-Si-Ali,S. (2014) The histone H3 lysine 9 methyltransferases G9a and GLP regulate polycomb repressive complex 2-mediated gene silencing. *Mol. Cell*, **53**, 277–289.
50. Rialdi,A., Campisi,L., Zhao,N., Lagda,A.C., Pietzsch,C., Ho,J.S.Y., Martinez-Gil,L., Fenouil,R., Chen,X., Edwards,M. *et al.* (2016) Topoisomerase 1 inhibition suppresses inflammatory genes and protects from death by inflammation. *Science*, **352**, aad7993.
51. Wang,J., Li,G.L., Ming,S.L., Wang,C.F., Shi,L.J., Su,B.Q., Wu,H.T., Zeng,L., Han,Y.Q., Liu,Z.H. *et al.* (2020) BRD4 inhibition exerts anti-viral activity through DNA damage-dependent innate immune responses. *PLoS Pathog*, **16**, e1008429.
52. Ferri,F., Petit,V., Barroca,V. and Romeo,P.H. (2019) Interplay between FACT subunit SPT16 and TRIM33 can remodel chromatin at macrophage distal regulatory elements. *Epigenetics Chromatin*, **12**, 46.
53. Daniel,B., Czimmerer,Z., Halasz,L., Boto,P., Kolostyak,Z., Poliska,S., Berger,W.K., Tzerpos,P., Nagy,G., Horvath,A. *et al.* (2020) The transcription factor EGR2 is the molecular linchpin connecting STAT6 activation to the late, stable epigenomic program of alternative macrophage polarization. *Genes Dev*, **34**, 1474–1492.
54. Chiappinelli,K.B., Strissel,P.L., Desrichard,A., Li,H., Henke,C., Akman,B., Hein,A., Rote,N.S., Cope,L.M., Snyder,A. *et al.* (2015) Inhibiting DNA methylation causes an interferon response in cancer via dsRNA including endogenous retroviruses. *Cell*, **162**, 974–986.
55. Izquierdo-Bouldstridge,A., Bustillos,A., Bonet-Costa,C., Aribau-Miralbes,P., Garcia-Gomis,D., Dabad,M., Esteve-Codina,A., Pascual-Reguant,L., Peiro,S., Esteller,M. *et al.* (2017) Histone H1 depletion triggers an interferon response in cancer cells via activation of heterochromatic repeats. *Nucleic Acids Res.*, **45**, 11622–11642.
56. Chen,Y.G. and Hur,S. (2022) Cellular origins of dsRNA, their recognition and consequences. *Nat. Rev. Mol. Cell Biol.*, **23**, 286–301.
57. Reilly,S.M., Chiang,S.H., Decker,S.J., Chang,L., Uhm,M., Larsen,M.J., Rubin,J.R., Mowers,J., White,N.M., Hochberg,I. *et al.* (2013) An inhibitor of the protein kinases TBK1 and IKK-varepsilon improves obesity-related metabolic dysfunctions in mice. *Nat. Med.*, **19**, 313–321.
58. Thomson,D.W., Poeckel,D., Zinn,N., Rau,C., Strohmer,K., Wagner,A.J., Graves,A.P., Perrin,J., Bantscheff,M., Duempelfeld,B. *et al.* (2019) Discovery of GSK8612, a highly selective and potent TBK1 inhibitor. *ACS Med. Chem. Lett.*, **10**, 780–785.
59. Liu,Y., Zhou,K., Zhang,N., Wei,H., Tan,Y.Z., Zhang,Z., Carragher,B., Potter,C.S., D'Arcy,S. and Luger,K. (2020) FACT caught in the act of manipulating the nucleosome. *Nature*, **577**, 426–431.
60. Hondele,M., Stuwe,T., Hassler,M., Halbach,F., Bowman,A., Zhang,E.T., Nijmeijer,B., Kotthoff,C., Rybin,V., Amlacher,S. *et al.* (2013) Structural basis of histone H2A-H2B recognition by the essential chaperone FACT. *Nature*, **499**, 111–114.
61. Hainer,S.J., Pruneski,J.A., Mitchell,R.D., Monteverde,R.M. and Martens,J.A. (2011) Intergenic transcription causes repression by directing nucleosome assembly. *Genes Dev.*, **25**, 29–40.
62. Roth,S.Y. and Allis,C.D. (1996) Histone acetylation and chromatin assembly: a single escort, multiple dances?*Cell*, **87**, 5–8.
63. Devaiah,B.N., Lewis,B.A., Cherman,N., Hewitt,M.C., Albrecht,B.K., Robey,P.G., Ozato,K., Sims,R.J. 3rd and Singer,D.S. (2012) BRD4 is an atypical kinase that phosphorylates serine2 of the RNA polymerase II carboxy-terminal domain. *Proc. Natl. Acad. Sci. U.S.A.*, **109**, 6927–6932.
64. Cha,T.L., Zhou,B.P., Xia,W., Wu,Y., Yang,C.C., Chen,C.T., Ping,B., Otte,A.P. and Hung,M.C. (2005) Akt-mediated phosphorylation of EZH2 suppresses methylation of lysine 27 in histone h3. *Science*, **310**, 306–310.
65. Wei,Y., Chen,Y.H., Li,L.Y., Lang,J., Yeh,S.P., Shi,B., Yang,C.C., Yang,J.Y., Lin,C.Y., Lai,C.C. *et al.* (2011) CDK1-dependent phosphorylation of EZH2 suppresses methylation of H3K27 and promotes osteogenic differentiation of human mesenchymal stem cells. *Nat. Cell Biol.*, **13**, 87–94.
66. Chen,S., Bohrer,L.R., Rai,A.N., Pan,Y., Gan,L., Zhou,X., Bagchi,A., Simon,J.A. and Huang,H. (2010) Cyclin-dependent kinases regulate epigenetic gene silencing through phosphorylation of EZH2. *Nat. Cell Biol.*, **12**, 1108–1114.
67. Tian,B., Yang,J., Zhao,Y., Ivanciuc,T., Sun,H., Garofalo,R.P. and Brasier,A.R. (2017) BRD4 couples NF-kappaB/RelA with airway inflammation and the IRF-RIG-I amplification loop in respiratory syncytial virus infection. *J. Virol.*, **91**, e00007–17.
68. Huang,B., Yang,X.D., Zhou,M.M., Ozato,K. and Chen,L.F. (2009) Brd4 coactivates transcriptional activation of NF-kappaB via specific binding to acetylated relA. *Mol. Cell Biol.*, **29**, 1375–1387.
69. Hargreaves,D.C., Horng,T. and Medzhitov,R. (2009) Control of inducible gene expression by signal-dependent transcriptional elongation. *Cell*, **138**, 129–145.
70. Wu,S.Y., Lee,A.Y., Hou,S.Y., Kemper,J.K., Erdjument-Bromage,H., Tempst,P. and Chiang,C.M. (2006) Brd4 links chromatin targeting to HPV transcriptional silencing. *Genes Dev*, **20**, 2383–2396.
71. McKinney,C.C., Kim,M.J., Chen,D. and McBride,A.A. (2016) Brd4 activates early viral transcription upon human papillomavirus 18 infection of primary keratinocytes. *Mbio*, **7**, e01644–16.
72. Yang,Z., Yik,J.H., Chen,R., He,N., Jang,M.K., Ozato,K. and Zhou,Q. (2005) Recruitment of P-TEFb for stimulation of transcriptional elongation by the bromodomain protein brd4. *Mol Cell*, **19**, 535–545.
73. Bisgrove,D.A., Mahmoudi,T., Henklein,P. and Verdin,E. (2007) Conserved P-TEFb-interacting domain of BRD4 inhibits HIV transcription. *Proc. Natl. Acad. Sci. U.S.A.*, **104**, 13690–13695.
74. Li,Z., Guo,J., Wu,Y. and Zhou,Q. (2013) The BET bromodomain inhibitor JQ1 activates HIV latency through antagonizing brd4 inhibition of Tat-transactivation. *Nucleic Acids Res.*, **41**, 277–287.
75. Niu,Q., Liu,Z., Alamer,E., Fan,X., Chen,H., Endsley,J., Gelman,B.B., Tian,B., Kim,J.H., Michael,N.L. *et al.* (2019) Structure-guided drug design identifies a BRD4-selective small molecule that suppresses HIV. *J. Clin. Invest.*, **129**, 3361–3373.
76. Conrad,R.J., Fozouni,P., Thomas,S., Sy,H., Zhang,Q., Zhou,M.M. and Ott,M. (2017) The short isoform of BRD4 promotes HIV-1 latency by engaging repressive SWI/SNF chromatin-remodeling complexes. *Mol. Cell*, **67**, 1001–1012.
77. Yigitliler,A., Renner,J., Simon,C., Schneider,M., Stubenrauch,F. and Iftner,T. (2021) BRD4S interacts with viral E2 protein to limit human papillomavirus late transcription. *J Virol.*, **95**, e02032–20.
78. Lam,F.C., Kong,Y.W., Huang,Q., Vu Han,T.L., Maffa,A.D., Kasper,E.M. and Yaffe,M.B. (2020) BRD4 prevents the accumulation of R-loops and protects against transcription-replication collision events and DNA damage. *Nat. Commun.*, **11**, 4083.
79. Sakamaki,J.I., Wilkinson,S., Hahn,M., Tasdemir,N., O'Prey,J., Clark,W., Hedley,A., Nixon,C., Long,J.S., New,M. *et al.* (2017) Bromodomain protein BRD4 is a transcriptional repressor of autophagy and lysosomal function. *Mol. Cell*, **66**, 517–532.
80. Jeanmougin,F., Wurtz,J.M., Le Douarin,B., Chambon,P. and Losson,R. (1997) The bromodomain revisited. *Trends Biochem. Sci.*, **22**, 151–153.
81. Kadota,S. and Nagata,K. (2014) Silencing of IFN-stimulated gene transcription is regulated by histone H1 and its chaperone TAF-I. *Nucleic Acids Res.*, **42**, 7642–7653.

82. McFarlane,S., Orr,A., Roberts,A.P.E., Conn,K.L., Iliev,V., Loney,C., da Silva Filipe,A., Smollett,K., Gu,Q., Robertson,N. *et al.* (2019) The histone chaperone HIRA promotes the induction of host innate immune defences in response to HSV-1 infection. *PLoS Pathog*, **15**, e1007667.
83. Gasparian,A.V., Burkhart,C.A., Purmal,A.A., Brodsky,L., Pal,M., Saranadasa,M., Bosykh,D.A., Commane,M., Guryanova,O.A., Pal,S. *et al.* (2011) Curaxins: anticancer compounds that simultaneously suppress NF-kappaB and activate p53 by targeting FACT. *Sci. Transl. Med.*, **3**, 95ra74.
84. Kim,M., Neznanov,N., Wilfong,C.D., Fleyshman,D.I., Purmal,A.A., Haderski,G., Stanhope-Baker,P., Burkhart,C.A., Gurova,K.V., Gudkov,A.V. *et al.* (2016) Preclinical validation of a single-treatment infusion modality that can eradicate extremity melanomas. *Cancer Res.*, **76**, 6620–6630.
85. Barone,T.A., Burkhart,C.A., Safina,A., Haderski,G., Gurova,K.V., Purmal,A.A., Gudkov,A.V. and Plunkett,R.J. (2017) Anticancer drug candidate CBL0137, which inhibits histone chaperone FACT, is efficacious in preclinical orthotopic models of temozolomide-responsive and -resistant glioblastoma. *Neuro Oncol.*, **19**, 186–196.
86. Carter,D.R., Murray,J., Cheung,B.B., Gamble,L., Koach,J., Tsang,J., Sutton,S., Kalla,H., Syed,S., Gifford,A.J. *et al.* (2015) Therapeutic targeting of the MYC signal by inhibition of histone chaperone FACT in neuroblastoma. *Sci. Transl. Med.*, **7**, 312ra176.
87. McKeown,M.R., Shaw,D.L., Fu,H., Liu,S., Xu,X., Marineau,J.J., Huang,Y., Zhang,X., Buckley,D.L., Kadam,A. *et al.* (2014) Biased multicomponent reactions to develop novel bromodomain inhibitors. *J. Med. Chem.*, **57**, 9019–9027.